Comparison of relaxation properties of collagen gel MRI phantoms at multiple magnetic fields

Olli-Pekka Aro
MSc thesis
Physics Degree Programme
Research Unit of Medical Imaging, Physics and Technology
University of Oulu
July 2020
Supervisor: Victor Casula

ABSTRACT

Osteoarthritis (OA) is the most common joint disorder in the world. OA affects the articular cartilage of synovial joints, causing disabilities and pain to those affected by the disease. The early stages of OA mainly affect the collagen and proteoglycan content of articular cartilage, causing it to lose its mechanical strength and start degrading. Magnetic resonance imaging (MRI) is a popular, non-invasive tool in OA diagnostics as it has the capability to detect morphological lesions and changes in the chemical composition of articular cartilage.

In this thesis, an MRI phantom study was designed and performed with the aim to investigate the effect of collagen and chondroitin sulfate (CS) concentration on the relaxation properties of gel-based phantoms at different magnetic field strengths. Three series of MRI phantoms as gels containing collagen and CS were made and dried to obtain final concentrations of collagen between 20-60 mg/g and CS between 0-40 mg/g. Three different relaxation properties were measured of the phantoms; R_1 and R_2 relaxation rates of the phantoms were measured at three different MRI field strengths (1.5, 3.0, and 9.4 T). Measurements at 1.5 and 3.0 T measurements were performed at Oulu University Hospital, while 9.4 T measurements were performed in Kuopio at the University of Eastern Finland. Additionally, $R_{1\rho}$ relaxation rates were measured at 9.4 T with multiple spin-lock frequencies.

From the measurements, it was determined that R_1 rates of the gels increased with the collagen concentration, while R_2 values were similar between the different series at lower magnetic fields but were noticeably higher and increased with increasing CS concentration at 9.4 T. $R_{1\rho}$ values increased with both collagen and CS content but the amplitude of the spin-lock pulse had next to no effect on the relaxation rates.

TIIVISTELMÄ

Nivelrikko on maailman yleisin nivelsairaus, joka vaikuttaa kantavien nivelten nivelrustoon, aiheuttaen kipua ja liikuntakyvyn sekä elämänlaadun heikkenemistä. Nivelrikon varhainen vaihe vaikuttaa pääasiassa nivelruston kollageeni- ja kondroitiinisulfaattipitoisuuteen, johtaen ruston mekaanisen vahvuuden ja kantokyvyn heikentymiseen ja lopulta ruston rappeutumiseen. Magneettikuvaus eli MRI on yksi suosituimmista nivelrikon diagnosointitavoista, sillä se kykenee havaitsemaan muutoksia ruston kemiallisessa rakenteessa ilman niveleen kajoamista esim. tähystysleikkauksen kautta.

Tässä opinnäytteessä kuvaillaan MRI-kuvantamisfantomitutkimusta, jonka päämääränä oli tutkia nivelruston olennaisimpien rakenneosien eli kollageenin ja kondroitiinisulfaatin konsentraatioiden vaikutusta relaksaationopeuteen erivahvuisissa magneettikentissä. Tutkimuksessa tehtiin kolme geelipohjaista MRI-fantomisarjaa, joissa kollageenin lopullinen konsentraatio vaihteli sarjan mukaan 20-60 mg/g välillä, kun taas kondroitiinisulfaatin konsentraatio oli 0-40 mg/g. Erilaisia magneettikuvauslaitteita käytettiin ulkoisen magneettikentän vahvuuden ja relaksaationopeuksien yhteyden selvittämiseksi; mittaukset 1.5 ja 3.0 Teslassa tehtiin Oulun yliopistollisessa sairaalassa, kun taas mittaukset 9.4 Teslassa suoritettiin Kuopiossa, Itä-Suomen yliopistossa. Kolme relaksaationopeutta mitattiin geeleistä; R_1- ja R_2-nopeudet mitattiin kolmessa erivahvuisessa magneettikentässä (1.5, 3.0 ja 9.4 T). Lisäksi $R_{1\rho}$-arvot mitattiin 9.4 Teslassa usealla “spin-lock” -taajuudella, jotta taajuuden amplitudin vaikutus relaksaationopeuteen saataisiin selville.

Tutkimuksen lopputuloksena saatiin, että geelien R_1-nopeudet kasvoivat lisääntyneen kollageenikonsentraation myötä. Toisaalta R_2-arvot olivat samankaltaisia keskenään heikommissa magneettikentissä konsentraatioista riippumatta, mutta olivat selvästi suurempia ja kasvoivat suurentuneen kondroitiinisulfaattikonsentraation myötä 9.4 Teslassa. $R_{1\rho}$-nopeudet kasvoivat sekä suurentuneen kollageeni- että kondroitiinisulfaattipitoisuuden myötä, mutta “spin-lock” -taajuudella ei ollut juurikaan vaikutusta nopeuksiin.

Acknowledgements

First, I would like to sincerely thank my thesis supervisor, Victor Casula, Ph.D., for the all the help and constant encouragement along these past few years, but especially during the process of writing this master thesis. I want to express my gratitude to Henning Henschel, Ph.D., formerly at the University of Oulu, currently at the University of Uppsala, for devising the research plan for this study and his great support and endless knowledge during the lab work phase. Furthermore, I would also like to thank the people who helped me with useful comments during the writing process of the article manuscript this thesis will hopefully become one day; acknowledgements go to Jouni Karjalainen, M.Sc., and professor Miika Nieminen, Ph.D., at the University of Oulu, and Nina Hänninen, M.Sc., and adjunct professor Mikko Nissi, Ph.D., at the University of Eastern Finland.

I would also like to give my heartfelt thanks to Docent Kyösti Heimonen, Ph.D., at NANOMO at the Faculty of Science for being the second reviewer of this master thesis. As my former boss and guiding teacher, his help and guidance have also been invaluable throughout my studies and I could count on his door being always open to me for anything.

I would like to especially thank my friends for all our times together during my studies; our study group Etkot for all the study sessions together in Tellus, Nuuti and V-J for all the banter, my former co-workers at the Transportation Centre at OYS for all the lunch breaks and ping pong matches, PP for the travelling and great conversations, to the boys at ÄMK, and finally, to my buddies at Pereily.

Finally, I am forever grateful to my mother and father for all their love and support throughout the years.

Olli-Pekka Aro
Oulu, 20.7.2020

Contents

List of Abbreviations and Symbols **vi**

1 Introduction **1**

2 Theory **4**

2.1 Articular cartilage 4

2.1.1 Collagen 5

2.1.2 Chondroitin sulfate 8

2.2 Magnetic resonance imaging 8

2.2.1 Nuclear magnetic resonance 9

2.2.2 Magnetization excitation and relaxation 11

2.2.3 Image acquisition 13

2.2.4 Longitudinal (T_1) relaxation 15

2.2.5 Transverse (T_2) relaxation 16

2.2.6 Spin echo 17

2.2.7 $T_{1\rho}$ relaxation 19

2.3 Literature research of relaxation in cartilage-like phantoms . . 22

3 Materials and Methods **25**

3.1 Phantom preparation 25

3.2 MRI measurements 27

4 Results **35**

5 Discussion **47**

Bibliography 52

List of Abbreviations and Symbols

3D	Three-dimensional
$\vec{M}_0$	Net magnetization vector
$\vec{M}_z$	Longitudinal component of net magnetization
$\vec{M}_{xy}$	Transverse component of net magnetization
B_0	Strength of external magnetic field
B_{SL}	Strength of spin-lock magnetic field
G_z	Strength of gradient field in z-direction
S_0	Signal intensity at equilibrium
CS	Chondroitin sulfate
CT	Computed tomography
dGEMRIC	Delayed gadolinium-enhanced MRI of cartilage
ECM	Extracellular matrix
FCD	Fixed-charge density
FSE	Fast spin-echo

GAG Glycosaminoglycan

Hz Hertz

IR Inversion recovery

MESE Multi echo spin-echo

MRI Magnetic resonance imaging

NMR Nuclear magnetic resonance

OA Osteoarthritis

PD Proton density

PG Proteoglycan

R_1 Spin-lattice relaxation rate ($=1/T_1$)

$R_{1\rho}$ Spin-lattice relaxation rate in the rotating frame ($=1/T_{1\rho}$)

R_2 Spin-spin relaxation rate ($=1/T_2$)

rf Radio frequency

ROI Region of interest

SAR Specific absorption rate

SD Standard deviation

SLF Spin-lock frequency

T Tesla

T_1 Spin-lattice relaxation time

$T_{1\rho}$ Spin-lattice relaxation time in the rotating frame

T_2 Spin-spin relaxation time

TE	Echo time
TR	Repetition time
TSE	Turbo spin-echo
TSL	Spin-lock time
α	Flip angle
γ	Gyromagnetic ratio
ω_0	Larmor frequency
ω_{SL}	Spin-lock frequency
$\vec{\mu}$	Magnetic dipole moment

Chapter 1

Introduction

Osteoarthritis (OA) is a highly debilitating illness that alters the structure of articular cartilage in the synovial joints. In recent years OA has affected particularly elderly and overweight people in increasing numbers [1], with approximately 27 million people affected in the United States [2]. It has been estimated that OA is the most common joint disorder in the world [3]. Currently the only effective treatment for the disease is total joint arthroplasty with a prosthetic replacement, which leads to rising costs in public healthcare as well as a considerable reduction in patients' quality of life [4].

Detecting early changes in content of the two main constituents in articular cartilage, collagen and chondroitin sulfate (CS), is crucial for diagnosing OA during the early onset of the disease. MRI is one of the most popular non-invasive methods for OA diagnostics, since it creates good contrast between different tissue types and the potential for detecting subtle changes in cartilage using MRI has improved in recent years. Conventional MR imaging uses the two main processes of relaxation: T_1 and T_2 relaxation. T_2 relaxation time mapping has been found to correlate with enzymatic degradation in cartilage, since it is influenced by water molecule mobility within the different tissue compartments [5] and also by the integrity and orientation of the collagen network and collagen fibres [6], [7], [8].

The main issue with using T_1- and T_2-mapping in OA diagnostics is that the relationship between soft tissue composition and *in vivo* relaxation times is still unclear. $T_{1\rho}$, or spin-lattice relaxation in the rotating frame, is considered to be promising in OA diagnostics. The main difference compared to T_1 and T_2 relaxation is that a $T_{1\rho}$ pulse sequence consists of an additional external, low-frequency RF pulse along the transverse plane after the initial 90° rf pulse, which "locks" the relaxing spins along its direction, leading to a slower relaxation process compared to T_2 relaxation [9]. $T_{1\rho}$ measurements at low spin-lock frequencies are especially adept at measuring low frequency interactions, such as between water and large molecules within the extracellular matrix (ECM) [10]. Changes in the ECM during OA, such as increases in water molecule movement [11], lead to increases in $T_{1\rho}$ values [12]. Correlation between collagen and/or PG concentration and T_2 values is still disputed. While some studies have found an association between them [13], with T_2 showing poor correlation with PG content in bovine cartilage compared to $T_{1\rho}$, while other studies found no correlation between T_2 times and PG content [12], [14]. However, $T_{1\rho}$ values do not correlate with collagen content [14]. T_1 mapping has been used in OA diagnostics using delayed gadolinium-enhanced MRI of cartilage (dGEMRIC), where charged contrast media is injected intravenously into the patient, which has been found to correlate with PG content in cartilage [15], [16].

The main purpose of this thesis was to prepare basic collagen and CS gel phantoms and investigate their ^{1}H relaxation properties. More specifically, the primary aims of this project were to study: (i) the concentration effect on R_1 ($= 1/T_1$), R_2 ($= 1/T_2$) and $R_{1\rho}$ ($= 1/T_{1\rho}$); (ii) the dependence of R_1 and R_2 relaxation rates on the main magnetic field strength; (iii) the effect of varying the spin-lock frequency on $R_{1\rho}$ relaxation rate. Furthermore, the secondary aim of this project was to compare R_2 relaxation rates measured using two different sequences: a fast echo spin-echo (FSE) and a multi-echo

spin-echo (MESE) sequence.

Chapter 2

Theory

2.1 Articular cartilage

Articular cartilage is a highly specialized type of connective tissue that covers the articulating ends of bones in the joints. Chondrocytes are the only cell type within cartilage which reside in the extracellular matrix (ECM). They are responsible for the upkeep and organization of the ECM. Chondrocytes amount to approx. 1-5 % of cartilage volume. Since articular cartilage lacks nerves, blood circulation or a lymphatic system, the only way chondrocytes obtain nutrients is through diffusion. The cartilage compresses and relaxes during different movement phases, which allows fluids to discharge and absorb through the tissue. The ECM consists of approx. 65-85 % water and solid components that mainly consist of collagen (15-20 %) and proteoglycans (PG) (3-10 %). In early OA the collagen structure of the ECM changes and PG content is reduced in the ECM, allowing water content to increase which causes the cartilage to lose its mechanical strength, leading to ECM eventually breaking down when collagen, water and PG content are reduced and the collagen fibre structure becomes severely altered. [11], [17], [18]

2.1.1 Collagen

Collagen is the most common protein among vertebrates. It is the main component of the ECM, accounting for 60-85 % of the dry weight in articular cartilage. Collagen molecules are unique in their structure, with three identical α-1-polypeptide chains forming together by interchain hydrogen bonds to create a triple helix structure around a common axis. The polypeptide chains consist of amino acids that are aligned in a repeating Gly-X-Y triplet, where glycyl is in every third position, while the X and Y positions are commonly vacated by proline and 4-hydroxyproline, respectively. The polypeptide chains and the triple helix structure are shown in detail in Figure 2.1. Several different types of collagen are found in cartilage, which can be classified as fibril-forming, network-forming, or transmembrane collagens, among others. The most common type of collagen found in articular cartilage is fibril-forming type II, which accounts for 80-95 % of all collagen in the ECM. [17], [18], [19], [20], [21]

In articular cartilage, type II collagen creates a fibrous network with cross-links with aggrecan molecules which provides the articular cartilage with mechanical strength and load bearing capabilities. The collagen fibre network is often divided into four distinctive layers; the superficial, middle (or transitional), radial (or deep) and calcified layers, respectively. The calcified zone is the transitional zone from the cartilage into the subchondral bone. In the radial zone nearest to the bone surface, the fibres are perpendicular to the cartilage surface, while in the middle zone the orientation of the fibres is random. In the topmost, superficial layer, the collagen fibres are packed densely and orientated parallel to the cartilage surface. The different layers are shown in Figure 2.2. The amount of collagen and PG vary between each zone, as well as the amount, size, and shape of chondrocytes. Collagen concentration decreases steadily from the surface of the cartilage to the deep zone. [17], [18], [19]

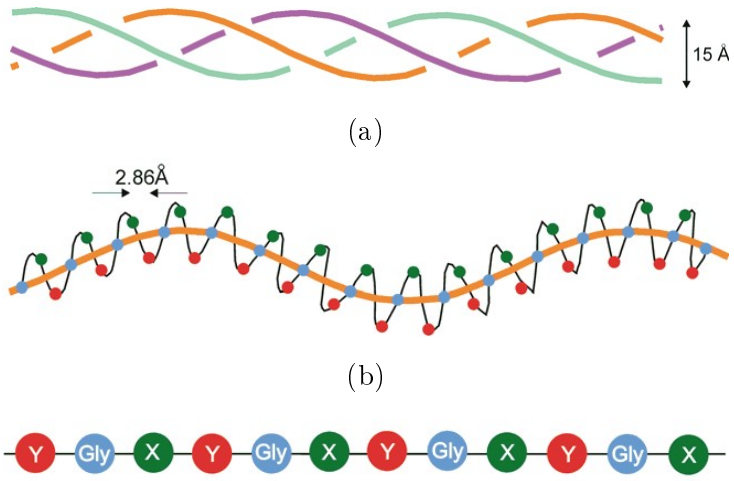

Figure 2.1: (a): The collagen triple helix. The size of the helix is 15 Å or 1.5 nanometers. The helix is characterised by the intertwining of three α-polypeptide chains. (b): Structure of an α-chain, with the amino acid sequence Gly-X-Y pattern repeating in the chains, which are connected to each other with hydrogen bonds. (c): X and Y spaces in the pattern are often vacated proline and hydroxyproline residues, respectively. Reprinted from [22].

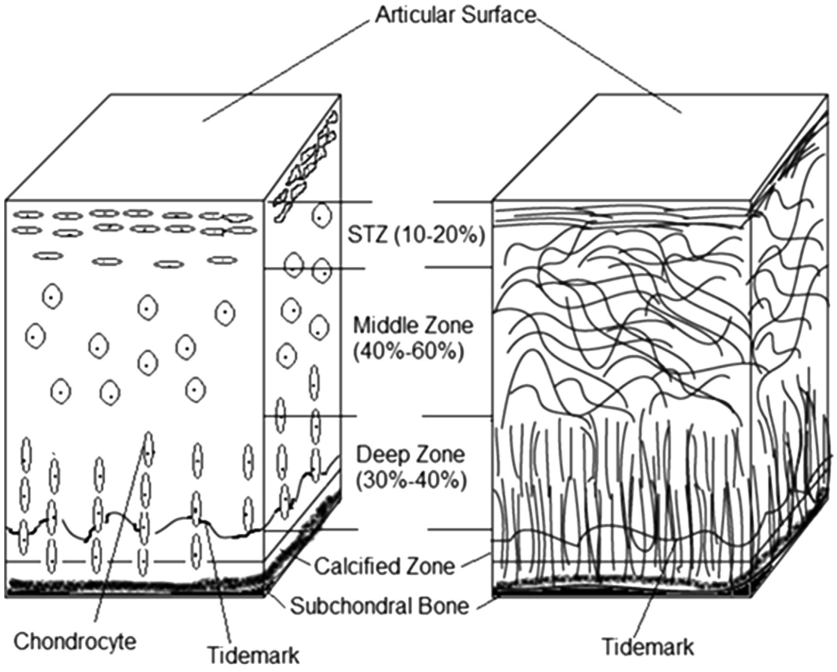

Figure 2.2: Articular cartilage divided into its histologic zones. The image depicts the cellular structure and collagen layer organization as well as the collagen fibre orientations. STZ = superficial zone. Reprinted from [24] with permission from Elsevier.

T_2 values in MRI images of samples containing collagen are dependent on their orientation and have a laminar appearance when orientated outside of the "magic angle". The magic angle effect is caused by the orientation of collagen fibres in an external magnetic field, because the water protons' interactions with collagen produce a non-averaging small dipolar magnetic field from each other. leading to anisotropy of T_2 values. The magic angle is given by the following equation:

$$3\cos^2\theta - 1 \tag{2.1}$$

where θ is the angle between the collagen fibrils and the external magnetic field. The anisotropy is vanished when the Equation 2.1 approaches zero, i.e. when θ approaches 54.74°. [23]

2.1.2 Chondroitin sulfate

Chondroitin sulfate (CS) is the most common glycosaminoglycan (GAG) in cartilage. GAGs are long, unbranched chains of polysaccharides, which consist of disaccharide units. The polysaccharides usually contain a sulfated group, which creates a negative charge to the GAG. GAGs form together with large core proteins to create proteoglycans (PG), the most abundant in cartilage being aggrecan. The structure of aggrecan is shown in Figure 2.3. Aggrecan's negative charge ties or "fixes" the molecule to the ECM, so they are often referred to as fixed-charge density (FCD). FCD is responsible for creating a concentration and charge difference between the tissue and the surrounding solution. This difference is known as Donnan osmotic pressure, which causes a driving gradient for water into the ECM. This makes the cartilage swell with water and the collagen fibres to be placed in tension to resist the swelling. The swelling makes PGs the controlling factors of the mechanical properties and the load-bearing capabilities of the cartilage, since such properties as elasticity and compressive stiffness of the tissue are highly linked with the amount of water in the ECM. The concentration of PGs vary in cartilage by location and the highest concentration of CS in is found in the middle zone (Figure 2.2). [17], [25], [26], [27]

2.2 Magnetic resonance imaging

Magnetic resonance imaging (MRI) is an imaging modality that uses nuclear magnetic resonance (NMR) in order to receive a signal from the body, instead of using ionizing radiation like other widely used imaging modalities such as conventional X-ray imaging and computed tomography (CT) do, or transmitting energy through tissue, like ultrasound does. NMR is based on interactions occurring within the atomic nucleus when it is subjected into an external magnetic field. The most commonly used nucleus in MRI is due to its abundance in nature and in tissue is hydrogen (^{1}H) which contains only a single proton, but other nuclei such as carbon (^{13}C), sodium (^{23}Na),

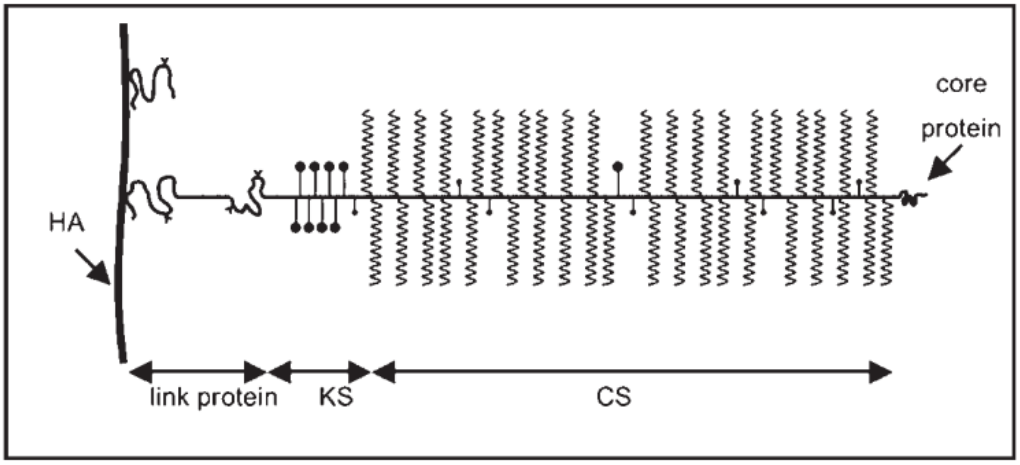

Figure 2.3: The structure of the aggrecan proteoglycan macromolecule composing of hyaluronic acid (HA), keratan sulfate (KS), and chondroitin sulfate (CS). Reprinted from [28] with permission from John Wiley and Sons.

and phosphorus (^{31}P) have be used. These following chapters focus on the interactions of hydrogen protons. [29], [30]

2.2.1 Nuclear magnetic resonance

The atomic nucleus is made of neutrons without a charge and protons with a positive charge, resulting in a net positive charge. Spin is a physical property of the nucleus that describes a form of internal angular momentum. In order for the nucleus to experience NMR, it must have a spin number that is non-zero. Spin is often portrayed as a proton spinning around its own axis that also has an electric charge. This electric charge creates a magnetic dipole moment $\vec{\mu}$ which aligns itself along an external magnetic field $\vec{B}_0$. Due to the electric charge within the nucleus, the proton experiences torque $\vec{\tau}$ when placed into a magnetic field:

$$\vec{\tau} = \vec{\mu} \times \vec{B} \tag{2.2}$$

The total number of protons and/or neutrons in the nucleus must be odd in order for the nucleus to have a magnetic moment, since an even amount of

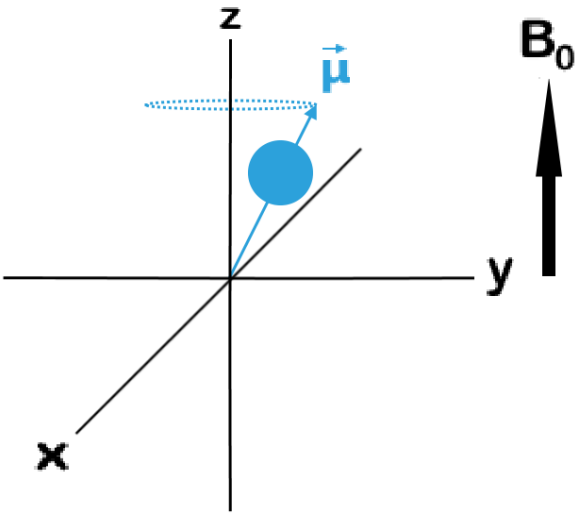

Figure 2.4: Precession of the magnetic dipole moment $\vec{\mu}$ along the z-axis.

nucleons causes the total magnetic moment to be zero. The torque imposed onto the protons by the magnetic field causes them to start precessing around the direction of the magnetic field axis at a constant angular frequency, shown in Figure 2.4. The frequency of precession is specific to the nucleus and called the Larmor frequency, which is given by the Larmor equation:

$$\omega_0 = \gamma B_0 \tag{2.3}$$

where γ is the gyromagnetic ratio and B_0 the strength of the magnetic field. Usually the frequency is given in SI units so the gyromagnetic ratio is divided by 2π, thus for hydrogen protons the gyromagnetic ratio $\frac{\gamma}{2\pi} = 42.58$ MHz T^{-1}. At 1.5 T, the Larmor frequency for hydrogen is 63.87 MHz, at 3.0 T 127.74 MHz, and at 9.4 T 400.25 MHz. [29], [30]

The magnetic moment in an external magnetic field is split into different energy states caused by the Zeeman effect. Since the spin quantum number m_s of a proton is $\frac{1}{2}$, it has two possible spin states; "spin-up" or parallel to the external field (spin quantum number $+\frac{1}{2}$), or "spin-down" or anti-parallel

to the magnetic field (spin quantum number $-\frac{1}{2}$). The energy difference of the two states is calculated using the following equation:

$$\Delta E = E_{-1/2} - E_{1/2} = \hbar\gamma B_0 = \hbar\omega_0 \tag{2.4}$$

where $E_{-1/2}$ is the energy of the "spin-down" state, $E_{1/2}$ the energy of the "spin-up" state, $\hbar$ is the reduced Planck constant ($= \frac{h}{2\pi}$), γ is the gyromagnetic ratio, B_0 the magnetic field strength, and ω_0 the Larmor frequency. The magnetic dipole moment vector of a proton does not fully align with the external magnetic field, because the protons have internal thermal energy, which is a much more significant factor in the alignment of the spins compared to the quantum spin energy. Quantum mechanically, the proton spins settle onto the two different quantum states and align either parallel or anti-parallel to the external magnetic field nearly equally according to the Boltzmann distribution, with only a few spins more per million spins aligning to the more stable, parallel energy state compared to anti-parallel, even in stronger magnetic fields. [29]

2.2.2 Magnetization excitation and relaxation

The collective amount of spins parallel to the external magnetic field create a net magnetization vector $\vec{M}$ which consists of components either parallel or perpendicular to the static main magnetic field. The external magnetic field is usually portrayed as being along the z-axis $\vec{B}_{ext} = B_0\hat{z}$, so the components of the magnetization vector are:

$$\vec{M} = M_{\parallel} + \vec{M}_{\perp} = M_z + M_x\hat{x} + M_y\hat{y} \tag{2.5}$$

where M_z is the magnetization along the longitudinal z-axis, M_x and M_y are magnetization in the transversal axes x and y, and $\hat{x}, \hat{y}$ and $\hat{z}$ are unit vectors of the respective axes in a rotating frame of reference that rotates around the z-axis at Larmor frequency. This is often chosen for portraying relaxation processes so that the motion of the spins would appear static at equilibrium and excitation. [29], [30]

The magnetization vector can be tipped away from equilibrium along the z-axis by transmitting a radio-frequency (rf) pulse using a transmitter coil close to the Larmor frequency of the protons. The rf pulse is a secondary magnetic field B_1 that has components perpendicular to the external magnetic field B_0. The rf pulse applies torque to the net magnetization, causing it to tip away from the z-axis and start precessing around the axis, shown in Figure 2.5. The angle that net magnetization is flipped to is called the "flip angle" which is given by the following equation:

$$\Delta\theta = \gamma B_1 \tau \tag{2.6}$$

where B_1 is the strength of the rf magnetic field (usually very small compared to B_0) and τ is the duration of the rf pulse which is usually in the millisecond range. The most common flip angles used in MR imaging are 90° (or a $\pi/2$ pulse) which tilts the magnetization to the transverse xy-plane, and 180° (π pulse) which flips the magnetization along the -z-axis. [29], [30], [31]

After the rf pulse, the net magnetization returns to its equilibrium along the external magnetic field. This process is called relaxation and the time it takes for the system to return to equilibrium is the relaxation time. There are two simultaneous relaxation processes happening in the system, spin-lattice or longitudinal relaxation (T_1), and spin-spin or transverse relaxation (T_2). The two processes are described mathematically using the Bloch equations [32]:

$$\frac{dM_z}{dt} = \frac{M_0 - M_z}{T_1} \tag{2.7}$$

$$\frac{dM_{xy}}{dt} = -\frac{M_{xy}}{T_2} \tag{2.8}$$

where M_0 is the value for net magnetization at equilibrium, M_z and M_{xy} are the longitudinal and transverse magnetizations, respectively, and T_1 and T_2 are longitudinal and transverse relaxation times, respectively. T_1 and

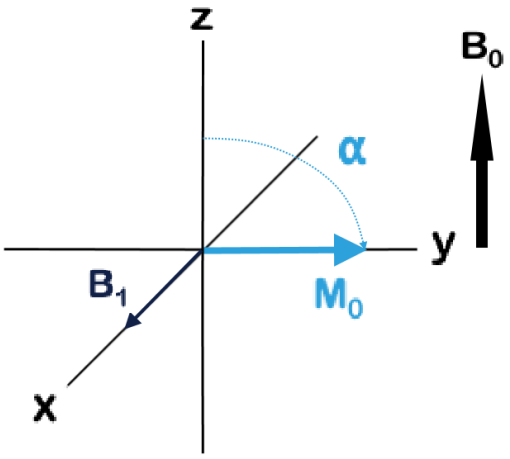

Figure 2.5: An rf pulse is applied along the x-axis. This produces an external magnetic field B_1 that tilts the net magnetization vector M_0 to the transverse plane. Here the flip angle α is $90°$.

T_2 relaxations are described in further detail in the following sections. Relaxation occurs at different rates specific to a tissue type, which creates contrast between the tissue types in MR images. [29], [30]

2.2.3 Image acquisition

A key concept of MRI is to spatially locate the NMR signal received from the sample. This is done by applying additional magnetic fields called gradient fields to the target. When a gradient field is switched on, the Larmor frequency and/or phase of the protons is varied slightly according to their position in the target. Three gradient fields are used in x-, y-, and z-directions, respectively, usually with the x-direction having a frequency-encoded gradient, y-directional gradients being phase-encoding, and the gradient field in the z-direction being the slice selection gradient. The frequency-encoding fields change the previously shown Equation 2.3 to the following form:

$$\omega_0(z) = \gamma\,(B_0 + z \cdot G_z) \tag{2.9}$$

where z is the position and G_z the strength of the gradient field in the z-direction, usually in the millitesla (mT) range. This makes the spatial differentiation of signals possible, as the Larmor frequency is now a function of location. [30], [31]

The imaging acquisition sequence starts by altering the frequency of the spins by turning on the gradient field in the z-direction (parallel to B_0) in order to select the position and thickness of the slice. The thickness of the slice is altered by changing either the strength of the gradient field or the bandwidth of the rf pulse. As the excitation rf pulse is switched on simultaneously with the gradient field, only the spins in the z-direction have their Larmor frequency changed, and spins in the xy-direction are, in theory, unaffected. [30], [31]

After the slice has been selected, the imaging data matrix containing the spatial frequencies called k-space is gathered from the slice. The data matrix is frequency-encoded in the x-direction (horizontally opposed to z-axis) and phase-encoded in the y-direction (vertically opposed to z-axis), meaning that each row alters by phase and each column by frequency from one another. When the phase-encoding gradient is turned on for a short moment, the spins precess either faster or slower depending on their position on the y-axis. After the gradient is turned off, the spins return to their original precession frequencies or speeds but the phase difference remains between the different positions as long as there is signal available ie. before the magnetization is decayed completely. When a gradient field in the x-direction is turned on, the frequencies within the selected slice are altered and the NMR signal is then measured and the information of the phases and/or frequencies are stored. Usually the k-space is gathered one row at a time between excitation pulses, since the signal decays rapidly. Acquisition time for two-dimensional experiments is dependent on the number of phase encoding steps:

$$T_{acq} = N_y \cdot TR \tag{2.10}$$

where N_y is the number of phase encoding steps (ie. rows in the image) and TR is the repetition time, or the time between excitation rf pulses. In case of three-dimensional imaging, the gradient field on the z-axis is turned into an additional phase-encoding axis and N_y is replaced in the previous equation by $N_y N_z$. This increases the image acquisition time even further, since additional lines are gathered, so additional excitations are required. [29], [30], [31]

The center of k-space contains the contrast of the image, while the peripheral regions contain the fine details of the structures, so if the k-space is not mapped fully, a high resolution image is not possible. After the k-space is gathered, the spatial frequencies that it holds are transformed into an image using inverse Fourier transform, which converts the MR signal from the frequency domain to the time domain. In case of a two-dimensional image, the inverse Fourier transform is portrayed by the following equation:

$$\hat{\rho}(x, y) = \int s(k_x, k_y) \exp(i2\pi k_x x + k_y y) dk_x \tag{2.11}$$

where the signal s_k is inverse Fourier transformed into an image which portrays the spin density $\rho(x, y)$ in each pixel. However, this is only in an ideal case, and in real-world experiments an estimate of the effective spin density $\hat{\rho}(x, y)$ is calculated. [29], [30], [31]

2.2.4 Longitudinal (T_1) relaxation

T_1 relaxation, also known as longitudinal or spin-lattice relaxation, describes the interaction between the spins and the surrounding lattice, as spins are in thermal contact with the surrounding lattice. This causes them to lose the energy gained from the rf pulse to their surroundings and return to equilibrium. Mathematically, T_1 relaxation describes the regrowth of longitudinal magnetization M_z and is described by the following equation:

$$M_z(t) = M_z(0) \exp(-t/T_1) + M_0(1 - \exp(-t/T_1)) \tag{2.12}$$

where t is time, $M_z(0)$ is the initial value for longitudinal magnetization at time = 0, and M_0 is the equilibrium value for net magnetization. T_1 is the

spin-lattice or longitudinal relaxation time, which is the amount of time required for 63 % of M_z to recover, as shown in Figure 2.6. T_1 is dependent on the tissue type and magnetic field strength and its values typically range between a few hundred and a few thousand milliseconds at 1.5 T. [29], [30], [31]

A common sequence for T_1 measurements is inversion recovery (IR), where the initial rf pulse is a 180° inversion pulse, which tilts the magnetization towards the -z-axis. Once the signal has recovered during a time period called inversion time (TI), a 90° pulse is applied and the magnetization is allowed to return to equilibrium. This has the advantage of producing a stronger T_1 signal, since the magnetization has to recover for a longer period compared to 90° pulses in order to return to equilibrium. In this thesis, an IR TSE (inversion recovery turbo spin-echo) sequence was used in T_1 measurements, where the IR sequence is combined with a turbo spin-echo sequence (discussed further in Section 2.2.6), allowing multiple images to be acquired with a single repetition. [30], [31]

2.2.5 Transverse (T_2) relaxation

T_2 relaxation, or transverse or spin-spin relaxation, describes the decay of the net magnetization vector's transverse component M_{xy}. Once a rf pulse is applied and the net magnetization is tipped to the transverse plane, the spins experience local fields that are combinations of the applied field and the fields of their neighbours. The variations in local fields cause the individual spins to fan out or "dephase" in time, reducing the transverse component of net magnetization vector. This process is shown in Figure 2.8. T_2 relaxation is given by the following equation:

$$M_{xy}(t) = M_{xy}(0)\exp(-t/T_2) \tag{2.13}$$

where $M_{xy}(0)$ is the transverse component of the net magnetization at time = 0, and T_2 is the spin-spin relaxation time, which is the time required for the

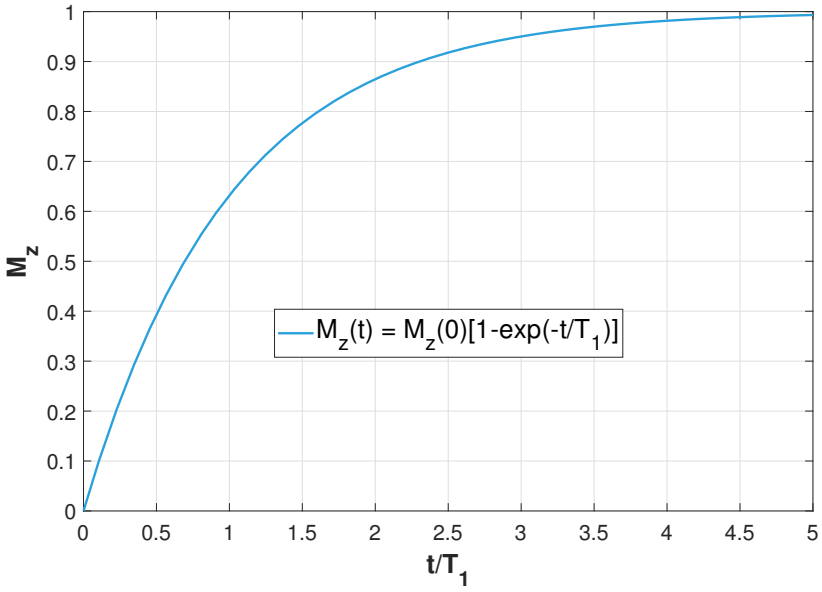

Figure 2.6: Illustration of T_1 relaxation made in Matlab by plotting Equation 2.12. As shown in the plot, when $t/T_1 = 1$, the longitudinal magnetization M_z has recovered approx. 63 % of the equilibrium value.

transverse relaxation to decay to approx. 37 % of its initial value, as shown in Figure 2.7. T_2 values are usually in the range of tens to a few hundred milliseconds, so T_2 is always shorter than T_1. T_2 is also less dependent on the strength of the external magnetic field compared to T_1 values. [29], [30]

2.2.6 Spin echo

In addition to internal dephasing, T_2 relaxation also contains additional dephasing due to inhomogeneities of the external magnetic field, that are portrayed by an additional time constant; T_2'. The total relaxation is the sum of both internal and external relaxation and portrayed by relaxation rate R_2^*, which is the reciprocal of relaxation times:

$$R_2^* = R_2 + R_2' = \frac{1}{T_2} + \frac{1}{T_2'} \tag{2.14}$$

where $T_2^* <= T_2$. Most of R_2^* consists of T_2' relaxation that can be reversed with an appropriate rf pulse. If the reversing pulse is applied after

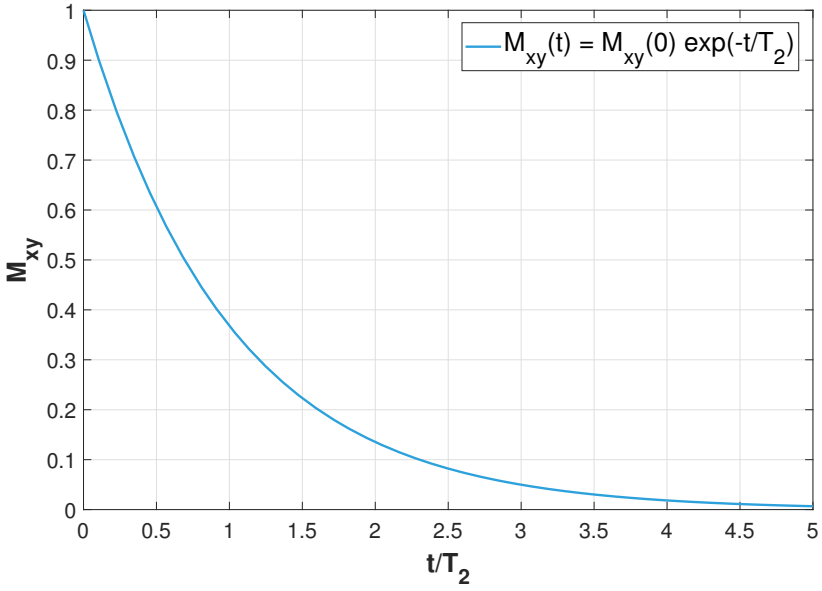

Figure 2.7: Illustration of T_2 made in Matlab by plotting Equation 2.13. As shown in the plot, when $t/T_2 = 1$, the transverse magnetization M_{xy} has decayed to approx. 37 % of its initial value.

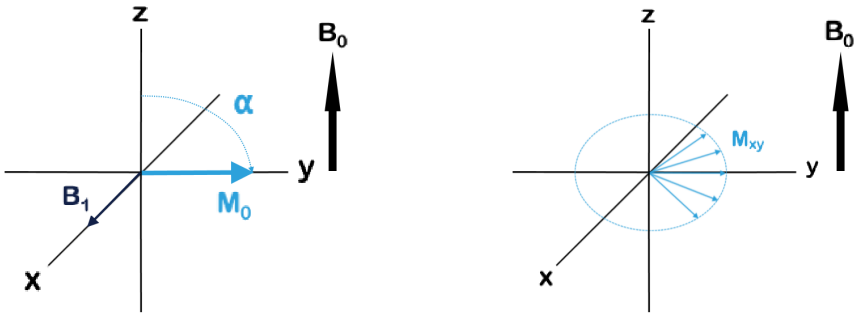

(a) (b)

Figure 2.8: Illustration of spin dephasing after a 90 degree rf pulse. (a): The 90° rf pulse tilts the net magnetization vector M_0 to the transverse plane. (b): The individual spins start to fan out and the transverse magnetization M_{xy} starts to decay.

the 90° pulse at a time period defined as τ, the reversing pulse causes the spins to flip around and rephase, causing a signal to be created at TE = 2τ. This process is called spin echo. An illustration of a spin echo sequence is shown in Figure 2.9. Multiple spin echoes can be measured during a single excitation period by producing additional rf pulses that flip the spins again. In this thesis, two different spin-echo sequences were used to measure T_2 values; a multi-echo spin-echo (MESE) and a fast echo spin-echo sequence (FSE). MESE sequences utilise an "echo train" which consists of multiple 180° refocusing pulses. When the echo train is applied to the target after an initial 90° pulse, an image can be measured with different T_2 weighting during a single echo train as long as sufficient T_2 relaxation exists. FSE sequences (also known as turbo spin-echo, TSE) differ from MESE sequences by utilising phase-encoding gradient fields, that switch on at the same time as 180° pulses. This allows FSE sequences to acquire multiple images with a single echo train, which allows them to have shorter scanning times, since less repetitions are required to scan the whole target. [29], [31]

2.2.7 $T_{1\rho}$ relaxation

Relaxation can also be measured in the presence of an additional rf pulse, as in $T_{1\rho}$ relaxation, or spin-lattice or longitudinal relaxation in the rotating frame. After the net magnetization is tipped to the transverse plane, a longer rf pulse called a spin-lock pulse (B_{SL}) is applied to the spins, some of which start revolving around the spin-lock field, similar to longitudinal relaxation revolving around the external magnetic field B_0. The frequency of the spin-lock pulse (SLF) ω_{SL} is calculated in a similar way to the Larmor frequency shown in Equation 2.3:

$$\omega_{SL} = \gamma B_{SL} \tag{2.15}$$

This process is shown in Figures 2.10 and 2.11. Similar to T_1 relaxation, as T_1 times increase with the strength of the external magnetic field B_0 [33], [34], [35], $T_{1\rho}$ relaxation times also increase with a stronger spin-lock pulse. However, longer spin-lock pulses can be an issue in *in vivo* imaging, as strict

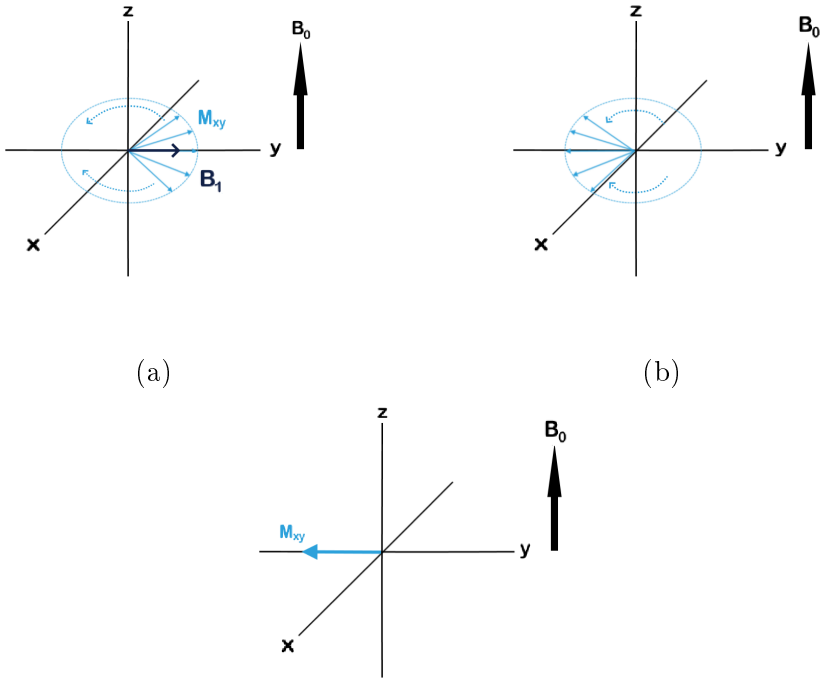

Figure 2.9: Illustration of the effect of the refocusing pulse on magnetization during a spin echo sequence. (a): At t = 0, right after the 90° rf pulse is applied to flip the magnetization to the transverse plane, the spins start to dephase due to the different precessing frequencies. (b): A 180° rf pulse applied at t = τ along the y-axis (π_y) flips the dephasing spins that start to rephase. (c): Spin echo signal is formed at t = 2τ = TE.

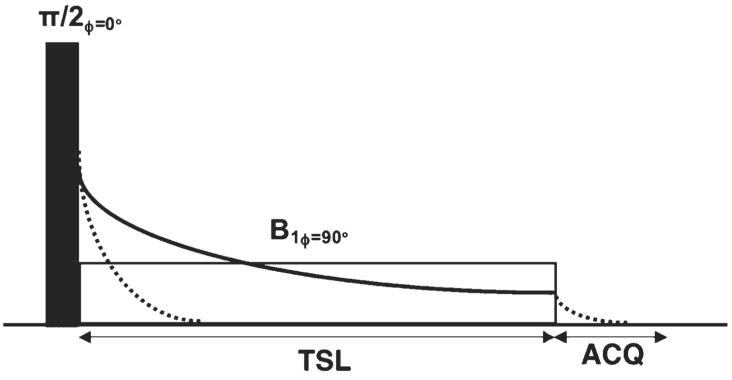

Figure 2.10: Pulse sequence for spin-locking magnetization to the transverse plane. A $\pi/2$ pulse (black rectangle) tilts the magnetization to the transverse plane, after which a spin-locking pulse (open rectangle) is applied. TSL is the duration of the pulse and B_1 its amplitude. The solid line represents $T_{1\rho}$ magnetization during the spin-lock pulse (duration TSL), while the dotted line represents the decay of magnetization (essentially T_2^* relaxation) without a spin-locking pulse. The spin-lock pulse slows the relaxation considerably. After the spin-lock pulse during the signal acquisition period (ACQ), the decay of the magnetization is again similar to T_2^* magnetization. Reprinted from [28] with permission from John Wiley and Sons.

limits are set on specific absorption rates (SAR) of energy deposited into the tissue, which increases with rf pulse power. In the $T_{1\rho}$ experiments of this thesis, ω_{SL} values between 50 and 1500 Hz were used. At low SLF, $T_{1\rho}$ relaxation times and/or relaxation rates ($=1/T_{1\rho}$) have been found to correlate with proteoglycan content in both bovine and human articular cartilage [14], [36], [37]. $T_{1\rho}$ is always longer than T_2, but shorter than T_1. [9], [28]

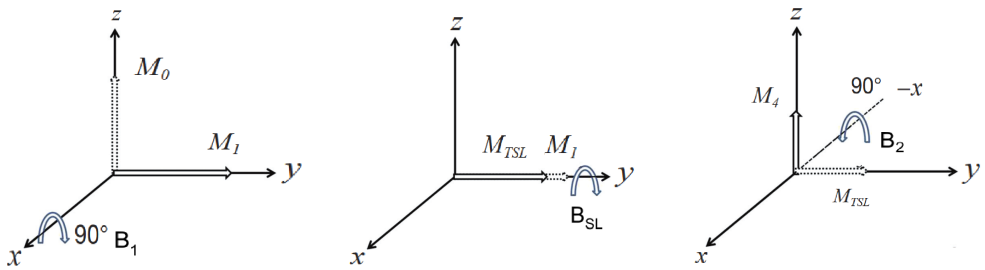

(a) (b) (c)

Figure 2.11: Diagram of magnetization evolution during a spin-lock sequence. (a): The 90° rf pulse tilts the net magnetization vector M_0 to the transverse plane. (b): The spin-lock pulse B_{SL} with a duration of TSL makes the magnetization M_1 rotate around itself along the y-axis, causing it simultaneously to slowly decay (portrayed by M_{TSL}). (c): Spin-locked magnetization M_{TSL} is finally flipped back to the longitudinal direction by a 90° pulse B_2 along the -x–axis and M_4 is measured. Reprinted from [9] with permission from Nancy International Ltd Subsidiary AME Publishing Company.

2.3 Literature research of relaxation in cartilage-like phantoms

A systematic literature search of previous studies regarding the relaxation properties of collagen gels or collagen MRI phantoms, and chondroitin sulfate and/or GAG suspensions was conducted for this thesis. This included searching for articles containing relevant keywords, such as “collagen gel”, “collagen phantom”, “chondroitin sulfate”, “NMR”, “MRI”, and “relaxation”, that were written in English published between 1950 and 2020 using multiple scientific search engines, including (alphabetically) Google Scholar, Oula-Finna, PubMed, Scopus, and Web of Science. The studies that were most relevant to this study are described in this section.

Several studies about the relaxation properties of collagen gels have been conducted. In one of the earliest studies of the subject, Westover and Dres-

den [38] studied the relaxation properties of native and denatured collagen gels and found that both T_1 and T_2 values decreased compared to pure water in low concentration collagen gels, with T_2 being the only value that changed depending on the structure of the gel. They also found that T_1 and T_2 values of denatured gels progressively decreased as collagen concentration increased. Edzes and Samulski [39] showed with proton NMR that R_1 values of hydrated collagen protons are mainly influenced by the macromolecular spin-lattice relaxation as a result of dipolar coupling between the water and macromolecular protons. Watanabe et al. [40] studied the effect of multi-slice acquisition on T_1 and T_2 measurements using collagen gels with added contrast agents, and found that both T_1 and T_2 values decreased with growing collagen concentration in single-slice measurements.

Takeuchi et al. [41] conducted a study about T_2 values of collagen gels at different orientations, and found that orienting the collagen fibres in the gels approx. 55° from the main magnetic field, eg. close to the "magic angle", increased their T_2 times at all concentrations. Kudo et al. [42] studied the connection states of collagen gels using T_1 and T_2 relaxation as parameters, among others. Some of the gels had collagen cross-links made with glutaraldehyde, which they found to affect the T_2 values proportionally to the glutaraldehyde concentration, while T_1 values of all gels were unaffected. Virta, Komu, and Kormano [43] investigated the $R_{1\rho}$ rates of protein solutions at "very low" magnetic fields ($B_0 = 0.1$ T, $B_1 < 200$ μT). While the magnetic field used was much smaller compared to the ones in this thesis, the study included a collagen solution at a similar concentration (50 mg/mL) to those used in this study. They found that $R_{1\rho}$ values "increased with increasing molecular content and concentration", but the used spin-lock fields were not suitable for determining the cause behind $R_{1\rho}$ values. Menezes et al. [13] studied T_2 and $T_{1\rho}$ values of articular cartilage systems of varying complexity, including pure suspensions of collagen and GAG of varying concentrations between 0-30 %, and found that both T_2 and $T_{1\rho}$ were approximately ex-

ponentially dependent on the concentration of both collagen or GAG, and that collagen concentration had a stronger effect on reducing either of the relaxation times.

Chapter 3

Materials and Methods

3.1 Phantom preparation

Three series of phantoms were made in which the final collagen concentrations of the gels varied between 20-60 mg/g, while CS concentrations were ranging from 0 to 40 mg/g (see Table 3.1).

Table 3.1: Phantom series with their collagen and chondroitin sulfate concentrations [mg/g], respectively.

Series	**Collagen concentration**	**CS concentration**
Samples 1-4	20	0, 10, 20, 40
Samples 5-8	40	0, 10, 20, 40
Samples 9-12	60	0, 10, 20, 40

The type I collagen used (Merck KGaA, Darmstadt, Germany) was extracted from rat tail and was delivered in an 0.01 M acetic acid solution (stock concentration: approx. 6 mg/mL). Chondroitin sulfate was a powder extracted from bovine trachea (Merck KGaA, Darmstadt, Germany). The initial gel was made by altering a manufacturer's (Ibidi, Gräfelfing, Germany) supplied collagen gel protocol [44]. The chondroitin sulfate powder was dissolved into

Table 3.2: Collagen, chondroitin sulfate, and total volumes [mL] of the samples before drying. CS values marked with an asterisk (*) used a CS solution with a stock concentration of 50 mg/mL, while all others used a solution of 80 mg/mL.

Series	**Collagen**	**CS**	**Total**
Samples 1-4	5	0, 0.1875, 0.375, 0.75	6
Samples 5-8	10	0, 0.30*, 0.60*, 0.75	11
Samples 9-12	15	0, 0.1875, 0.375, 0.75	16

a water solution, with the stock concentration of the CS solution being adjusted to 50-80 mg/mL. The phantom was made by placing all substances on ice, before pipetting collagen into a tube, with the amount being dependent on the final concentration. 10x phosphate buffered saline (PBS), CS and double distilled water (ddH_2O) were added into the collagen solution. The amount of 10x PBS added was constant in all tubes, with the amount being 0.15 mL which was one tenth of the final, dried gel. The volumes of the gels before the drying process are shown in Table 3.2. After all substances had been added, the sample was thoroughly mixed and pH was checked with indicator paper. pH was adjusted to be approximately neutral or slightly basic (approx. 7-9) using 1 M sodium hydroxide (NaOH) and 0.5 M hydrochloric acid (HCl), in order for the sample to solidify properly.

Once the collagen mixtures were neutralized, they were placed into a warm water bath at 37 °C in order to solidify the mixture into a gel. The samples were initially kept in the bath for 45-60 minutes, after which the gels were checked for their solidity. The pH adjustment and incubation was repeated for the samples, if it was deemed necessary. After the gels were solid, they were removed from their tubes and then transferred into a plastic cell culture dish, which was placed into a laminar flow oven. The temperature of the oven was 40 °C. The samples were covered with a large dish in such a way

that airflow would only be one way, from under the samples. This raised the collagen and CS concentrations to the levels by removing the excess water from the samples. The samples were kept in the oven until the final mass of each sample was reduced to approx. 1.5 grams, after which they were placed into small plastic tubes for MRI measurements.

3.2 MRI measurements

The samples were measured using a 1.5 T (Siemens Magnetom Aera, Germany) and a 3 T (Siemens Magnetom Skyra, Germany) MRI scanner, in combination with a 15 channel transmit/receiver coil (QED, Mayfield Village, OH, USA) at Oulu University Hospital. Three-dimensional images of the samples were obtained using a 3D proton density weighted (SPACE) sequence. T_1 values were measured using an inversion recovery turbo spin echo (IR TSE) sequence, while T_2 values were measured with two different sequences; a fast spin echo (FSE) sequence and a multi-echo spin echo sequence (MESE/MapIT). The pulse sequence parameters used in 1.5 and 3.0 T measurements are shown in Table 3.3. A MR image of the samples is shown in Figure 3.1.

The measurements of T_1, T_2, and $T_{1\rho}$ at 9.4 T were performed at the University of Eastern Finland with a 9.4 T MRI scanner (Oxford instruments Plc, Witney, UK) in combination with a 19-mm quadrature volume RF transceiver (RAPID Biomedical GmbH, Rimpar, Germany) and VnmrJ3.1 Varian/Agilent DirectDrive console. Pulse sequences parameters used in the 9.4 T measurements are shown in Table 3.4.

Slices of the best quality were selected from the MR images by determining their locations from three-dimensional images and appropriate regions of interest (ROI) were drawn on the slices MR images using a Matlab-based program (Aedes, University of Eastern Finland, Kuopio, Finland, `http`:

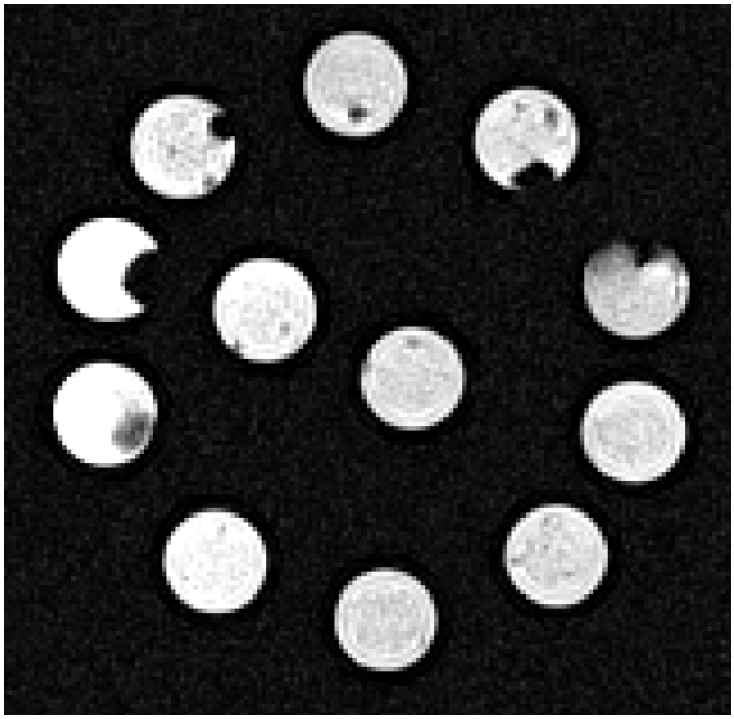

Figure 3.1: MR image of the gel samples at 1.5 T acquired with a FSE sequence.

`//aedes.uef.fi`). The ROIs were drawn so that they were in approximately the same locations for all three measurements by matching the positions of the multi-slice setups between the 1.5, 3.0, and 9.4 T measurements. This was done by calculating the distance of the slice from the bottom of the phantom. A sample of the ROIs drawn onto the maps is shown in Figure 3.2. In all measurements, T_1 and T_2 maps of the phantoms were calculated using in-house written plugins for Aedes, by fitting the image intensities voxel-wise to a mono-exponential decay model in order to create a two-dimensional relaxation time map. The equations for the mono-exponential decay model are shown in Equations 3.1 and 3.2:

$$S(t) = S_0(1 - 2\exp(-\mathrm{TI}/T_1)) \tag{3.1}$$

$$S(t) = S_0 \exp(-\mathrm{TE}/T_2) \tag{3.2}$$

where S_0 is the intensity of the original signal, TI is the inversion time and TE is the echo time. In the 9.4 T measurements, $T_{1\rho}$ maps were created by using the Witschey sequence [45] and making two-parameter fits of the raw data, with the $T_{1\rho}$ map using Equation 3.3:

$$S(t) = S_0 \exp(-\mathrm{TSL}/T_{1\rho}) \tag{3.3}$$

where TSL is the spin-lock time. The final values used were weighted averages of the different slices' fitted data with zero-value voxels removed, using the pixel count of each ROI as the weighing factor. The standard deviations of the final values were pooled from the slices' values using Equation 3.4:

$$SD_{pooled} = \sqrt{\frac{(n_1 - 1) \cdot {SD_1}^2 + (n_2 - 1) \cdot SD_2^2 + \ldots + (n_k - 1) \cdot SD_k^2}{(n_1 + n_2 + \ldots + n_k)}} \tag{3.4}$$

where n_k is the pixel count and SD_k is the standard deviation of the slice k. Aedes was used to obtain the relaxation times from the maps within the previously determined ROIs. The measured map data was then transferred to Microsoft Excel for averaging and to Matlab for plotting.

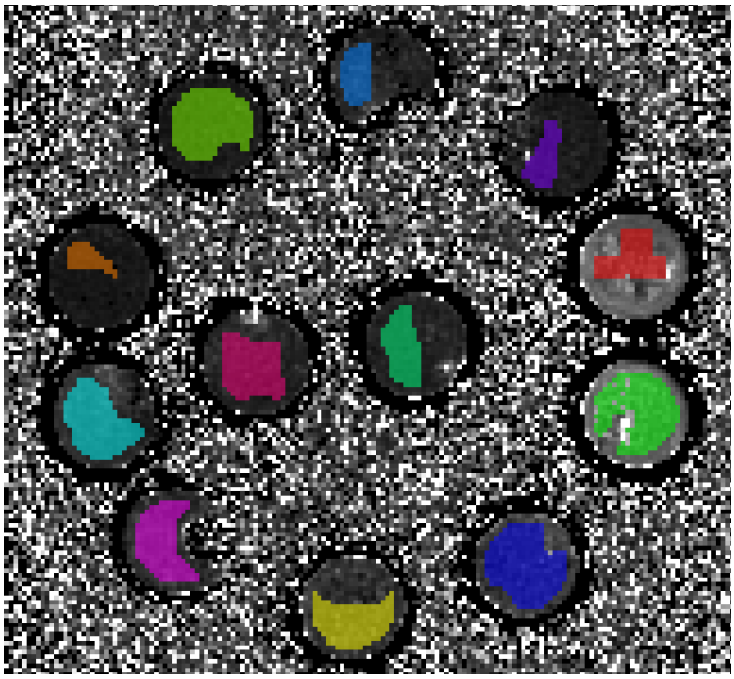

Figure 3.2: A T_2 relaxation time map of the samples with the ROIs drawn onto the map.

Table 3.3: Pulse sequence parameters for the 1.5 T and 3.0 T measurements.

Sequence	**Parameters**
3D PD SPACE	Resolution = 0.5x0.5x0.5 mm^3 TR = 1200 ms TE = 26 ms Flip angle = 120° No. of slices = 72 No. of averages = 2 ETL = 55 BW = 425 Hz/pixel
T_1 IR TSE	Resolution = 0.4x0.4x2.0 mm^3 TR = 10000 ms TI = 400, 800, 1600, 3200, 7000, 9000 ms No. of slices: = 7 No. of averages = 2 Interslice gap = 1 mm

Table 3.3 – continued from previous page	
T_2 FSE	Resolution = 0.4x0.4x2.0 mm^3 TR = 10000 ms TE = 12, 23, 35, 47, 58, 70, 93, 120, 180, 286, 320, 440, 841 ms No. of slices = 7 No. of averages = 2 Interslice gap = 1 mm
T_2 MESE	Resolution = 0.4x0.4x2.0 mm^3 TR = 10000 ms TE = 12, 24, 36, 48, 60, 72, 84, 96, 108, 120, 132, 144, 156, 168, 180, 192, 250, 300, 350, 400, 450, 500, 550, 600, 650, 700, 750, 800 ms No. of slices = 7 No. of averages = 2 Interslice gap = 1 mm

PD = proton density, ETL = echo train length, MESE = multi-echo spin-echo, FSE = fast spin-echo, TI = inversion time, TE = echo time, TR = repetition time, TSL = spin-lock time.

Table 3.4: Pulse sequence parameters for the 9.4 T measurements.

Sequence	**Parameters**
T_1 IR FSE	Resolution = 0.4x0.4x2.0 mm^3 TR = 10000 ms ESP = 5 ms ETL = 8 with centric echo ordering No. of averages = 1 Interslice gap = 1 mm TI = 400, 800, 1600, 3200, 5000, 7000 and 9000 ms
T_2 FSE	Resolution = 0.4x0.4x2.0 mm^3 TR = 10000 ms ESP = 5 ms ETL = 8 with centric echo ordering No. of averages = 1 Interslice gap = 1 mm TE = 0, 10, 20, 40, 80, 160, 320 and 640 ms
T_2 MESE	Resolution = 0.4x0.4x2.0 mm^3 TR = 10000 ms ESP = 5 ms ETL = 8 with centric echo ordering No. of averages = 1 Interslice gap = 1 mm TE = 12-768 ms, in increments of 12 ms

Table 3.4 – continued from previous page	
T1ρ	Resolution = 0.4x0.4x2.0 mm^3 TR = 10000 ms ESP = 5 ms ETL = 8 with centric echo ordering No. of averages = 1 Interslice gap = 1 mm SLF = 50, 100, 150, 200, 300, 400, 600, 800, 1000, 1500 Hz TSL = 0, 10, 20, 40, 60, 80, 100, 200 and 400 ms

ESP = echo spacing, ETL = echo train length, MESE = multi-echo spin-echo, FSE = fast spin-echo, TI = inversion time, TE = echo time, TSL = spin-lock time.

Chapter 4

Results

As presented in Table 4.1 and Figures 4.1 and 4.2, generally R_1 relaxation rates decreased with increasing magnetic field strength. The effect was more clearly seen in the samples with the highest collagen content, as shown in Figure 4.1. R_1 values seemed to slightly increase with the collagen concentration, as the 60 mg/g collagen concentration series had the highest relaxation rates at all magnetic fields, with the 20 and 40 mg/g series' values being similar to each other. In the 9.4 T measurements the differences in R_1 values were the smallest. No obvious increase was seen in R_1 values with increasing CS concentration in the sample series. Most of sample series had some increases with the concentration at 1.5 and 3.0 T, compared to the 9.4 T measurements where no apparent relation between the two could be seen.

R_2 values measured with a MESE sequence (Table 4.2 and Figures 4.4) showed that the values themselves were significantly higher at 9.4 T compared to the lower magnetic fields, as shown in Figure 4.3. Standard deviations of the values were relatively larger in the 9.4 T measurements compared to the other magnetic fields used. R_2 values were very similar between the different collagen series at the lower magnetic fields, with no apparent increase in values seen in Figure 4.4 regardless of collagen concentration. At 9.4 T however, the differences between series came forth, with R_2 values of

Table 4.1: Mean values and standard deviations of the R_1 relaxation rates [s^{-1}] of the gel phantoms.

B_0	collagen/CS [mg/g]	0	10	20	40
1.5 T	20	0.49 ± 0.02	0.51 ± 0.04	0.53 ± 0.03	0.55 ± 0.04
	40	0.53 ± 0.03	0.57 ± 0.03	0.57 ± 0.03	0.62 ± 0.04
	60	0.61 ± 0.04	0.59 ± 0.05	0.68 ± 0.05	0.77 ± 0.09
3.0 T	20	0.37 ± 0.01	0.47 ± 0.10	0.46 ± 0.10	0.45 ± 0.09
	40	0.40 ± 0.05	0.43 ± 0.08	0.46 ± 0.09	0.57 ± 0.02
	60	0.54 ± 0.06	0.53 ± 0.08	0.57 ± 0.03	0.59 ± 0.03
9.4 T	20	0.40 ± 0.00	0.43 ± 0.01	0.39 ± 0.01	0.42 ± 0.02
	40	0.44 ± 0.01	0.41 ± 0.01	0.42 ± 0.01	0.50 ± 0.01
	60	0.46 ± 0.02	0.48 ± 0.02	0.46 ± 0.02	0.50 ± 0.03

the higher collagen concentration series being noticeably larger. The values showed an apparent increase in R_2 values with the increasing CS concentration in the 20 mg/g collagen series at all magnetic field strengths and in the 40 mg/g series at 9.4 T (Figure 4.3), but a similar effect was not seen in the higher collagen concentrations. The only increase in the higher series was between the samples with and without CS, but the amount of added CS didn't seem to affect R_2 values. At 1.5 and 9.4 T however, a nearly linear increase could be seen in the 20 and 40 mg/g series with the increasing CS content, with the increase being steeper at the higher magnetic field.

The differences in R_2 values between MESE (Table 4.2 and Figures 4.3 and 4.4) and FSE (Table 4.3 and Figures 4.5 and 4.6) sequences are relatively large especially in the 3.0 T measurements. Using a MESE sequence, R_2 values are nearly the same at 3.0 T and 1.5 T, whereas in the FSE measurements, 3 T values are noticeably lower compared to 1.5 T in all sample series. The different sequences' differences include the magnitudes of errors in the values of the 9.4 T measurements, with FSE having larger errors compared to MESE. Also, the R_2 values of the MESE measurements at the lower magnetic fields

Table 4.2: Mean values and standard deviations of the R_2 relaxation rates [s^{-1}] of the gel phantoms measured with a multi-echo spin-echo (MESE) imaging sequence.

B_0	collagen/CS [mg/g]	0	10	20	40
1.5 T	20	1.69 ± 0.14	2.41 ± 0.44	3.54 ± 0.62	3.34 ± 0.62
	40	1.75 ± 0.17	5.13 ± 0.51	4.90 ± 0.60	4.86 ± 0.51
	60	5.11 ± 0.65	3.12 ± 0.49	4.74 ± 0.59	4.77 ± 0.66
3.0 T	20	1.70 ± 0.14	2.28 ± 0.33	3.13 ± 0.49	3.44 ± 0.55
	40	1.77 ± 0.30	4.33 ± 0.59	4.16 ± 0.61	4.38 ± 0.63
	60	5.16 ± 0.73	2.92 ± 0.57	5.01 ± 0.55	4.86 ± 0.87
9.4 T	20	3.46 ± 0.20	4.52 ± 0.48	4.97 ± 1.17	5.66 ± 1.24
	40	3.23 ± 0.24	5.76 ± 0.46	8.49 ± 0.82	9.21 ± 1.29
	60	11.89 ± 1.38	8.89 ± 1.47	11.08 ± 1.68	13.47 ± 2.65

are closer to each other within the different series, as seen in Figures 4.4 and 4.6. R_2 values at 3.0 T are noticeably higher in the MESE sequence measurements compared to FSE values.

$R_{1\rho}$ relaxation rates were only measured at 9.4 T due to a lack of a sequence that was suitable for the measurements on the Siemens scanners. The rates are shown in Figures 4.7 and 4.8. The relaxation rates increased with collagen concentration. The same effect is seen with increasing CS concentration as well, with the relaxation rates following the increasing CS concentration. The only exception to this was the 60 mg/g collagen sample without any CS, which had higher $R_{1\rho}$ values compared to the lower CS concentration samples. However, below 60 mg/g the differences between $R_{1\rho}$ values of the different CS concentration series got larger as the collagen concentration increased. The spin-lock frequency did not seem to have much of an effect on $R_{1\rho}$ relaxation rates, with only slight dispersion showing in all of the series. However, the dispersion is only happening below 50-100 Hz, after which most of the series reach a plateau. Increasing collagen and/or CS makes the relaxation dispersion somewhat steeper.

Table 4.3: Mean values and standard deviations of the R_2 relaxation rates [s^{-1}] of the gel phantoms measured with a fast spin-echo (FSE) imaging sequence.

B_0	collagen/CS [mg/g]	0	10	20	40
1.5 T	20	2.44 ± 0.31	3.11 ± 0.57	3.95 ± 0.66	3.85 ± 0.62
	40	2.58 ± 0.36	4.72 ± 0.69	4.57 ± 0.67	4.52 ± 0.66
	60	4.63 ± 0.73	3.65 ± 0.66	4.65 ± 0.77	4.72 ± 0.79
3.0 T	20	0.88 ± 0.10	1.33 ± 0.23	1.74 ± 0.33	1.69 ± 0.31
	40	0.87 ± 0.13	2.31 ± 0.37	1.79 ± 0.29	2.34 ± 0.28
	60	2.87 ± 0.55	1.61 ± 0.31	3.09 ± 0.61	3.04 ± 0.69
9.4 T	20	2.25 ± 0.96	3.53 ± 0.83	5.47 ± 1.62	6.22 ± 2.18
	40	3.07 ± 1.31	5.90 ± 1.79	8.61 ± 2.31	10.90 ± 2.58
	60	14.43 ± 3.97	11.36 ± 4.33	11.05 ± 2.07	14.13 ± 3.80

Since the Witschey -off-resonance $T_{1\rho}$ pulse sequence that was used contains a refocusing pulse in the middle of the spin-lock sequence [45], the measurements with SLF = 0 Hz were effectively using the same sequence as T_2 FSE measurements. However, the R_2 values measured with a FSE sequence are not as similar as one would expect to those with the Witschey sequence, with R_2 values being either higher or lower with the FSE sequence. All values still were in the range of errors of the values. The R_2 values obtained at SLF = 0 were all slightly higher compared to R_2 MESE measurements at 9.4 T shown in Figure 4.4.

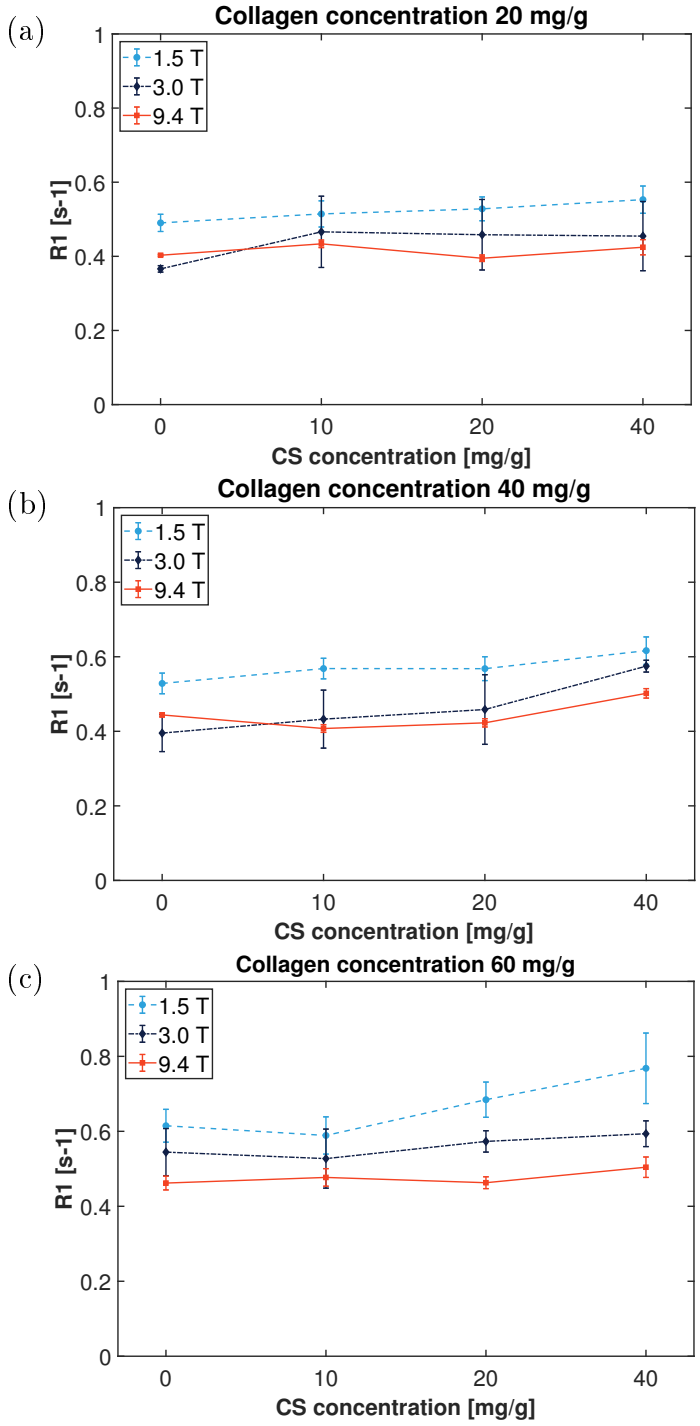

Figure 4.1: R_1 values of the different series at different magnetic fields shown as a function of CS concentration with collagen concentration being 20 mg/g (a), 40 mg/g (b), and 60 mg/g (c). Error bars indicate standard deviations.

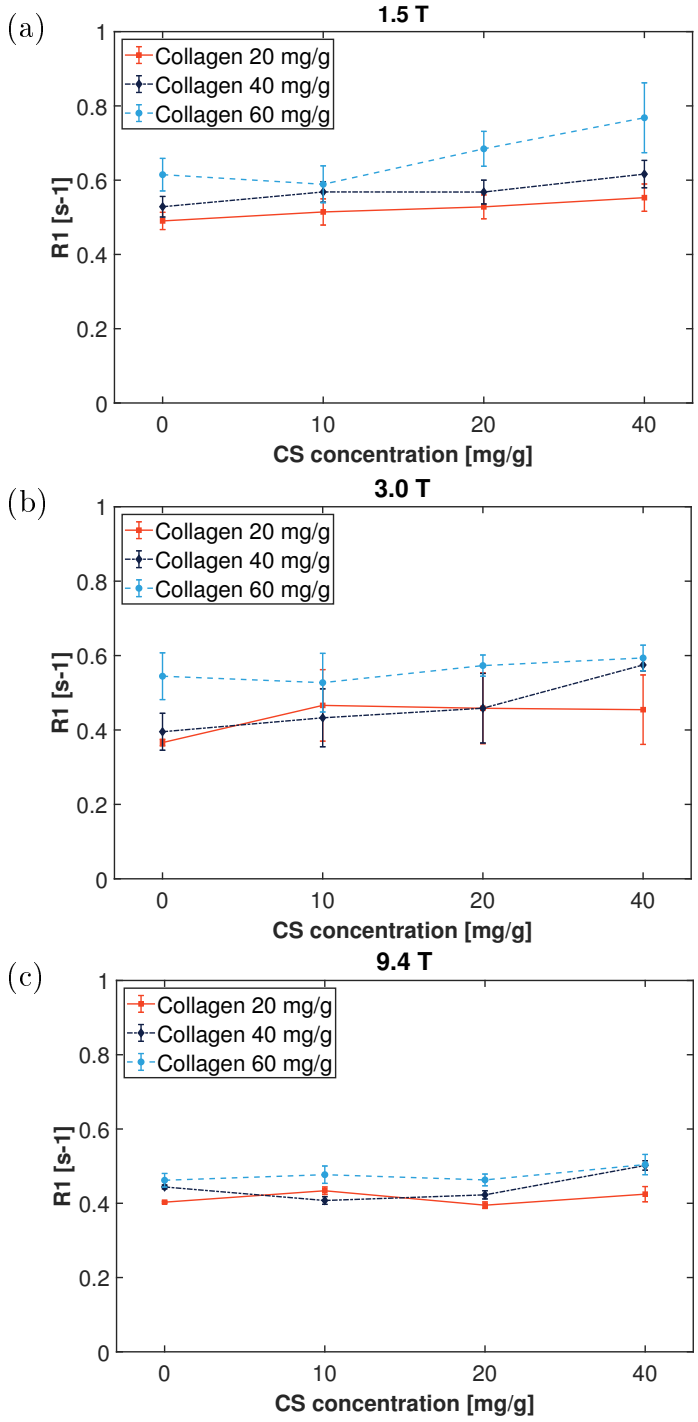

Figure 4.2: R_1 values as a function of CS concentration at 1.5 T (a), 3.0 T (b), and 9.4 T (c). Error bars indicate standard deviations.

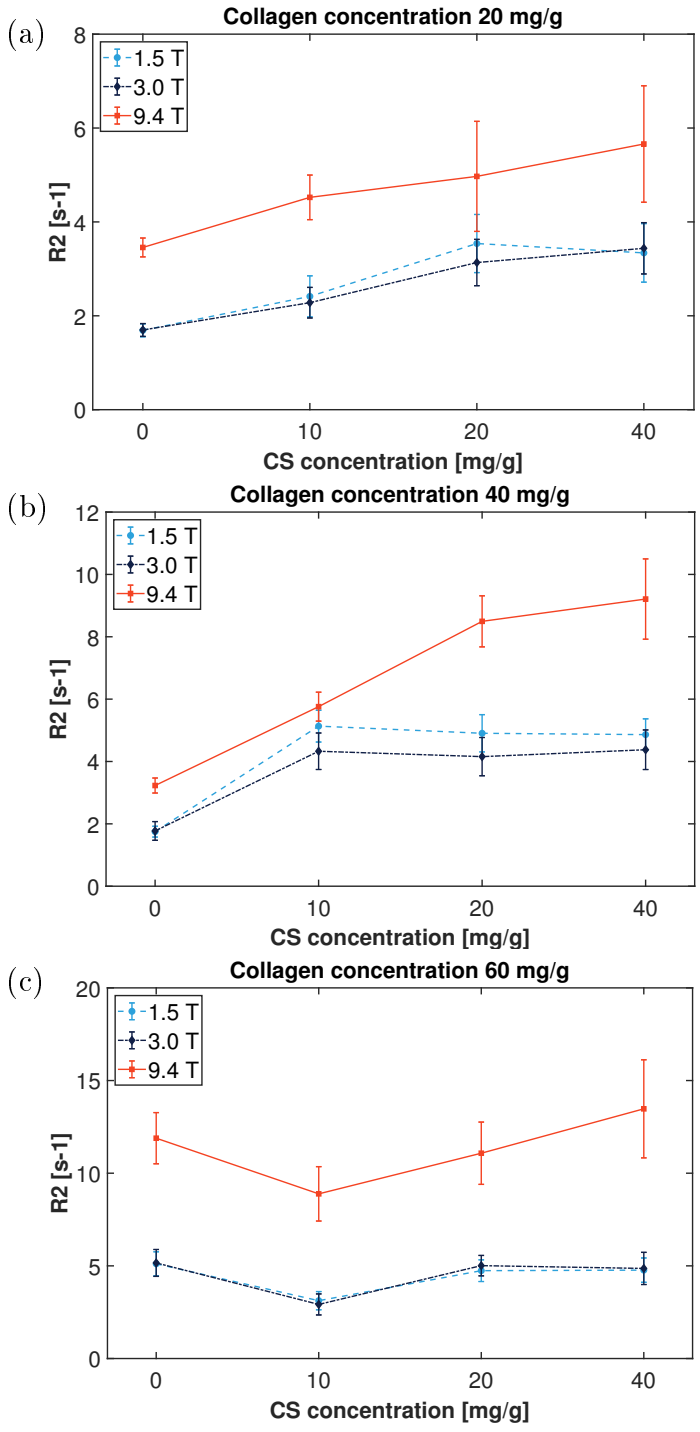

Figure 4.3: R_2 values measured with a multi-echo spin-echo (MESE) sequence as a function of CS concentration with collagen concentration being 20 mg/g (a), 40 mg/g (b), and 60 mg/g (c). Error bars indicate standard deviations.

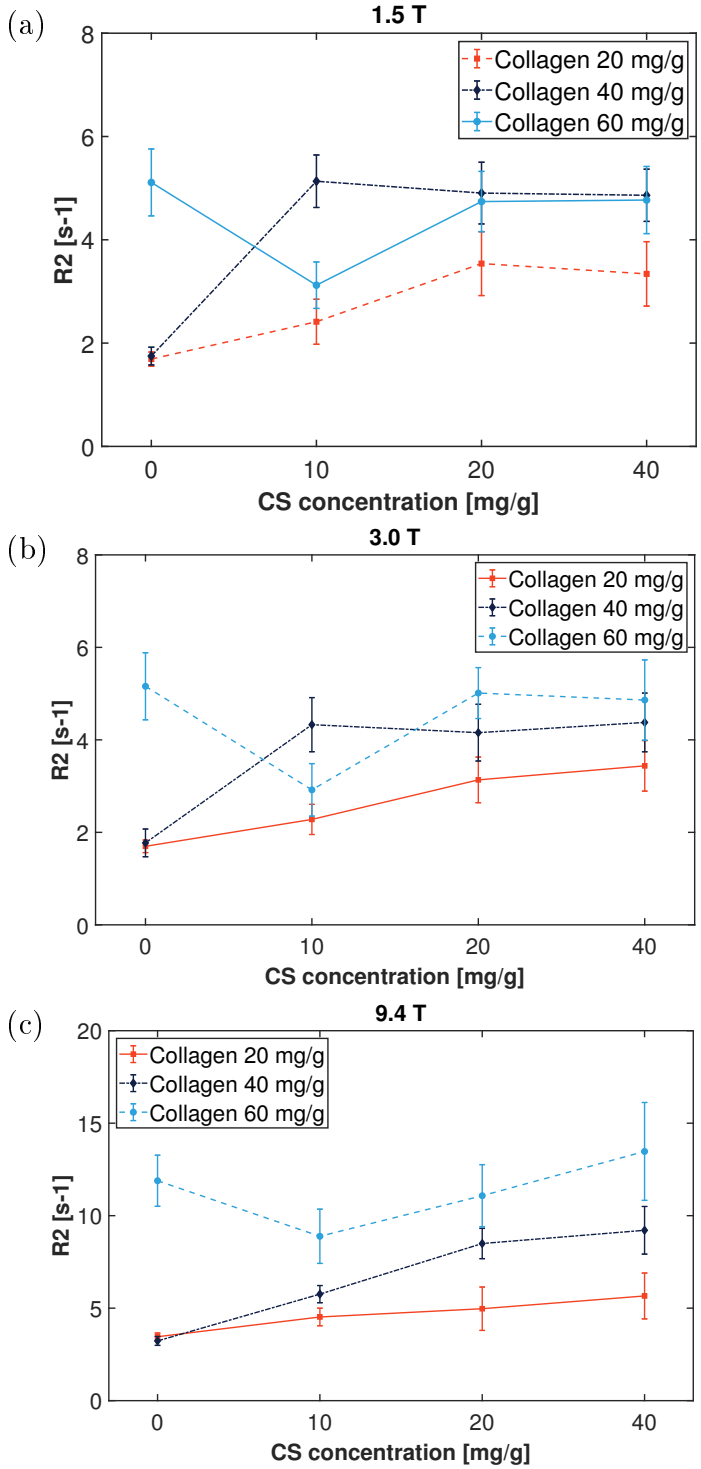

Figure 4.4: R_2 values measured with a multi-echo spin-echo (MESE) sequence as a function of CS concentration at 1.5 T (a), 3.0 T (b), and 9.4 T (c). Error bars indicate standard deviations.

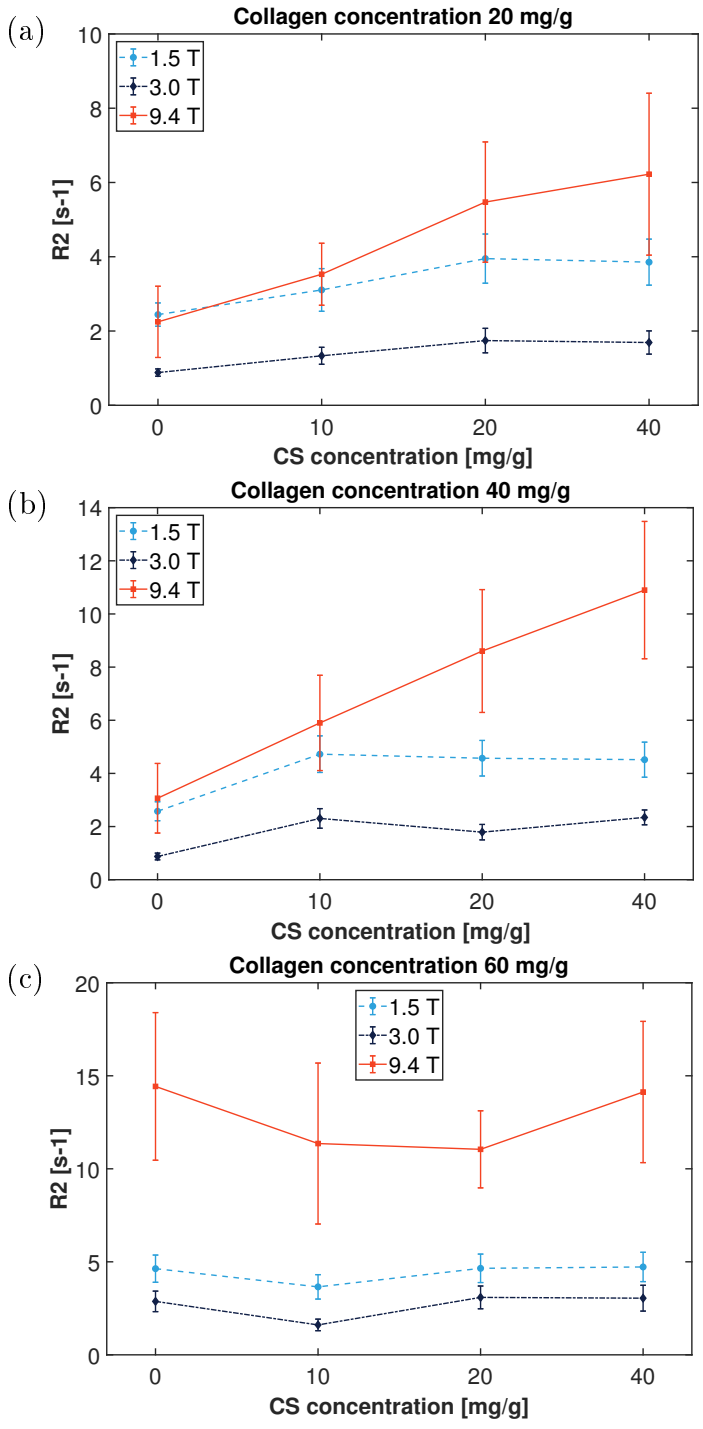

Figure 4.5: R_2 values measured with a fast spin-echo (FSE) sequence as a function of CS concentration with collagen concentration being 20 mg/g (a), 40 mg/g (b), and 60 mg/g (c). Error bars indicate standard deviations.

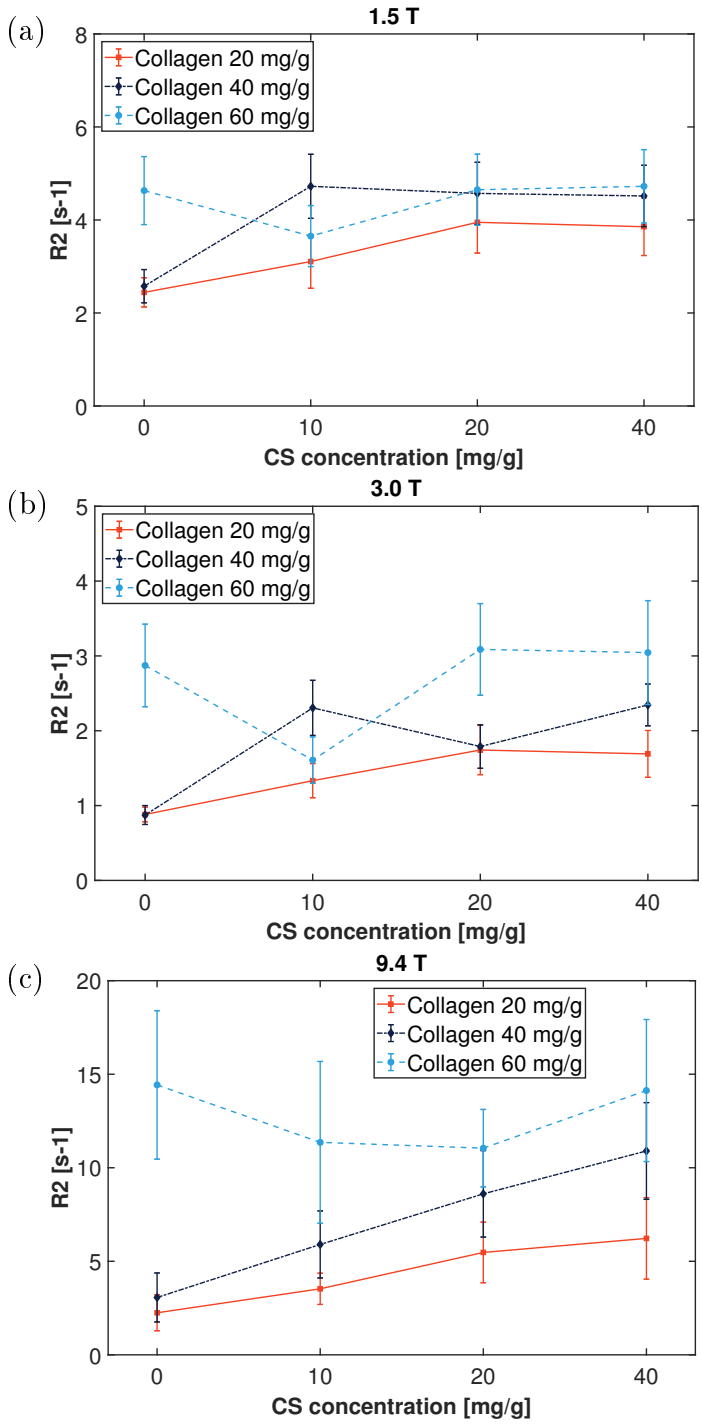

Figure 4.6: R_2 values measured with a fast spin-echo (FSE) sequence as a function of CS concentration at 1.5 T (a), 3.0 T (b), and 9.4 T (c). Error bars indicate standard deviations.

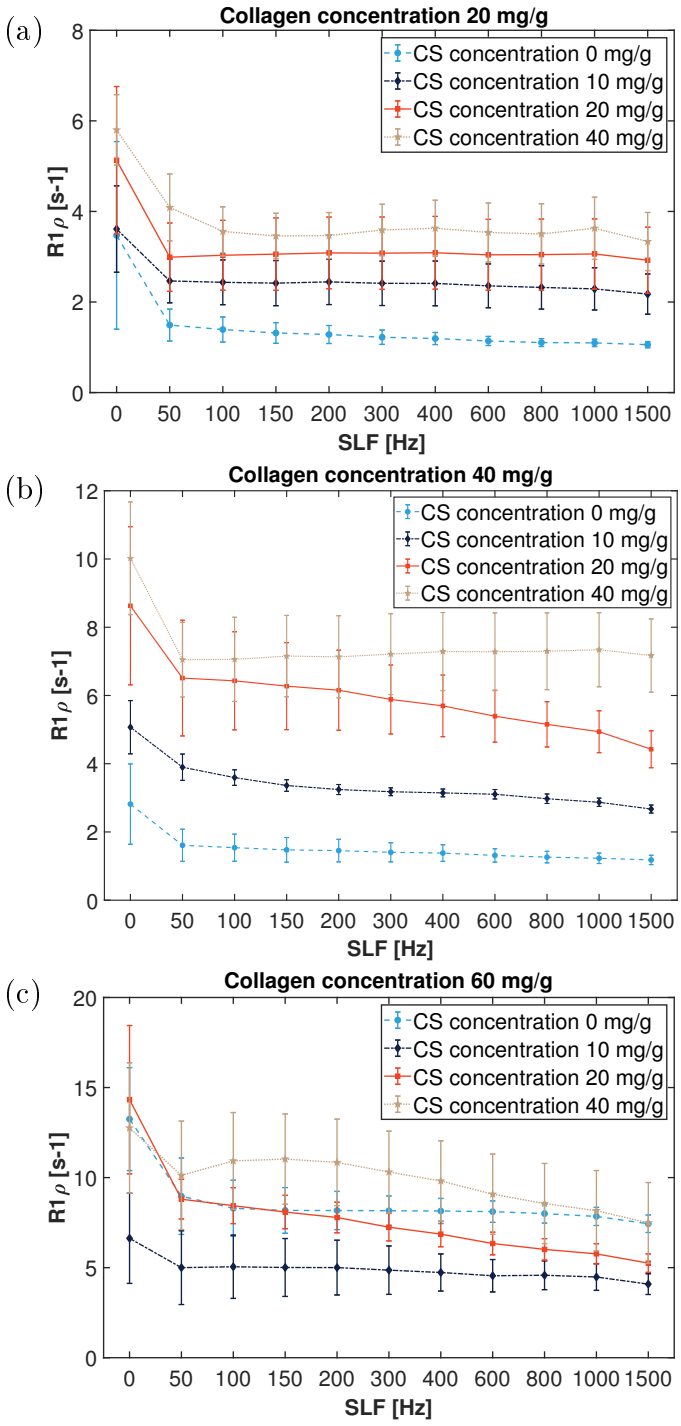

Figure 4.7: $R_{1\rho}$ relaxation rates of the different sample series as a function of spin-lock frequency (SLF) with collagen concentration being 20 mg/g (a), 40 mg/g (b), and 60 mg/g (c). Error bars indicate standard deviations.

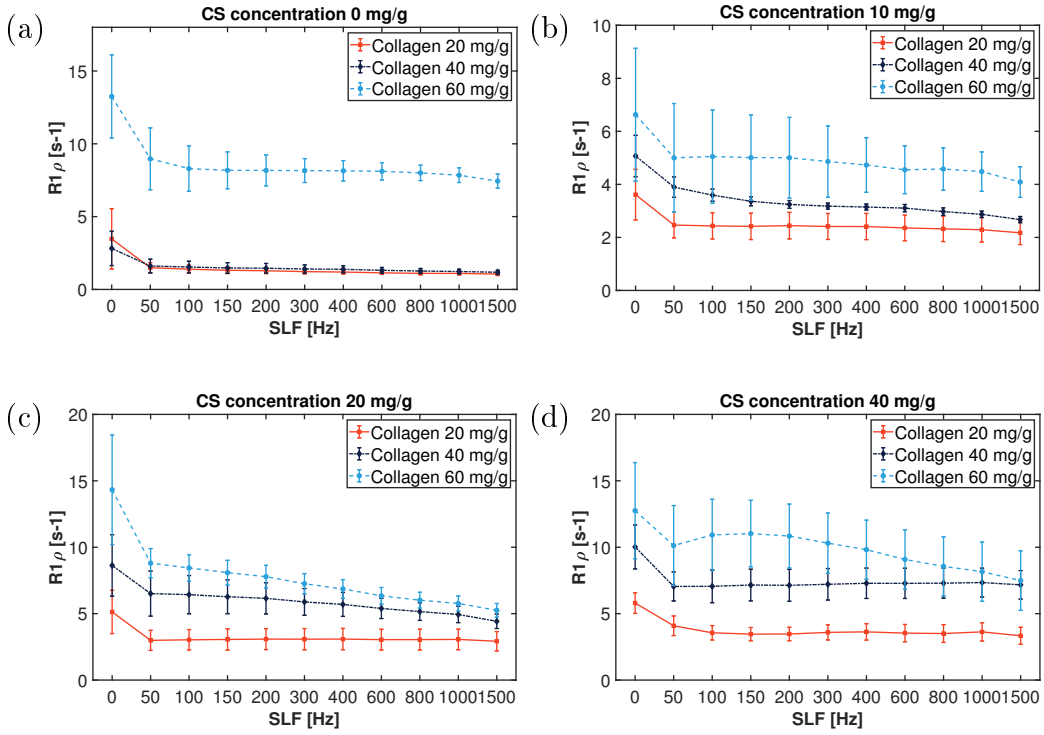

Figure 4.8: $R_{1\rho}$ relaxation rates of the different CS concentrations as a function of spin-lock frequency (SLF) with CS concentration being 0 mg/g (a), 10 mg/g (b), 20 mg/g (c), and 40 mg/g (d). Error bars indicate standard deviations.

Chapter 5

Discussion

In this thesis, MRI imaging phantoms were created which only contained the most important components of articular cartilage, collagen and chondroitin sulfate. The main findings from MRI measurements indicate that R_1 values generally increased with increasing collagen concentration at all magnetic field strengths, R_2 values increased with the CS concentration in the series with the lowest collagen concentration, suggesting that the effect of collagen on relaxation is dominant at higher concentrations. R_2 only increased with the collagen concentration at high magnetic fields while $R_{1\rho}$ values increased with collagen and CS concentration in nearly all sample series. Moreover, in this study the manufacturing process of collagen gels is described more accurately compared to previous studies, while also raising the collagen and CS concentrations higher compared to similar phantom studies without using a centrifuge. This is an important detail as centrifuging will be more costly and difficult to use compared to the basic lab equipment used in our study. The concentrations of either collagen or CS were higher in this study compared to previous collagen gel phantom studies mentioned in Section 2.3, with only a single exception, with collagen concentrations ranging between 2.5 and 280 mg/mL in the aforementioned studies. However, concentrations in our phantoms did not reach the levels that occur *in vivo*, as according to Westover and Dresden [38], a collagen concentration of 30 % (300 mg/g)

would be “comparable to the collagen content of tendon”.

R_1 relaxation rates decrease with increasing the magnetic field strength, as predicted by relaxation theories and experimentally observed previously [33], [34], [35]. However, the rise of R_2 values at 9.4 T compared to the lower magnetic fields was unexpected. This could indicate that the R_2 measurements at different magnetic field strengths are not directly comparable to each other, since different equipment and sequences were used. Also, the differences between the different sequences used in R_2 measurements were larger than expected, so those results were not comparable to each other either. Additionally, the sample with concentrations of 60 mg/g collagen and 10 mg/g CS has lower values in all R_2 and $R_{1\rho}$ measurements compared to the other 60 mg/g samples, suggesting a possibility of this sample being an outlier with air bubbles affecting the different values.

The phantoms had their collagen concentrations raised significantly from the stock concentration of the solution by drying them in a laminar flow oven. The collagen and CS concentration of cartilage however, is still much higher than we managed to reach in our experiments, with one study estimating the mean concentrations of collagen and CS in canine cartilage being 198.9 ± 34.1 mg/mL and 89.7 ± 28.5 mg/mL, respectively [46]. Using a multiple linear regression estimation of the relaxation data, a rough prediction of the relaxation rates at concentrations closer to ones in cartilage could be calculated and the estimates of R_1 and R_2 rates are shown in Figure 5.1. While the R_1 extrapolation shown in Figure **??** (as $T_1 \approx 460$ ms) would be quite close to some of the values of “in vivo” cartilage T_1 at 1.5 T shown in [47], it should be taken with caution, since the extrapolation was made from only a few data points that are far from the actual values. The R_2 extrapolation in Figure **??** (as $T_2 \approx 22.6$ ms) was not as close to actual T_2 values at 9.4 T shown in [48].

It seems that the range of spin-lock frequencies used in this study doesn't

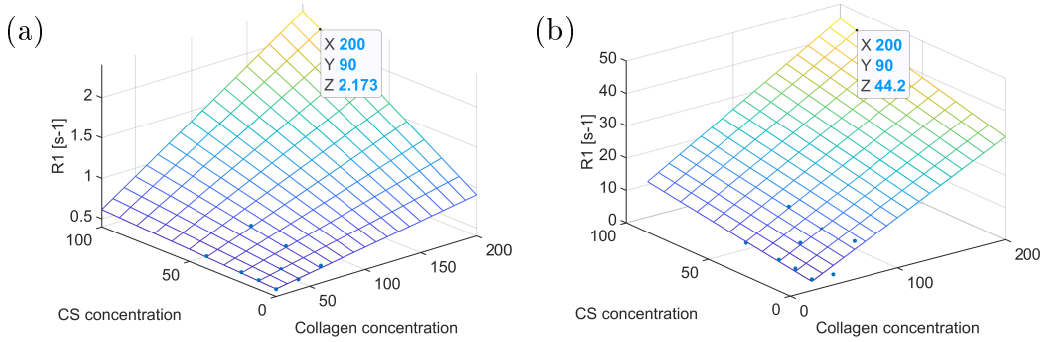

Figure 5.1: Results from a multiple linear regression model that was used to extrapolate the measured relaxation rates to higher concentrations of collagen and CS, which would be closer to concentrations naturally occurring in cartilage. (a): R_1 rates extrapolated from 1.5 T data, $R^2 = 0.9286$. (b): R_2 rates extrapolated from 9.4 T data, $R^2 = 0.8494$.

have much influence on the $R_{1\rho}$ values. A dispersive effect that has been previously seen in some *ex vivo* cartilage $T_{1\rho}$ experiments, such as [36] and [37], is missing in our experiment in the lower concentrations entirely. This suggests that there must be another effect than dispersion which affects the relaxation rates. However, the mentioned studies used either different spin-lock frequencies or studied different systems so similar results wouldn't necessarily be expected from our study. No previous comparable studies researching $T_{1\rho}$ properties in collagen gel systems at high magnetic fields were found. Only one previous study by Virta, Komu, and Kormano [43] was found that studied $T_{1\rho}$ properties of collagen solutions, albeit at much lower magnetic fields, so their results are not directly comparable to ours. The underlying effect in cartilage causing dispersion in the $R_{1\rho}$ is still unclear. Mlynárik et al. [49] measured $R_{1\rho}$ in their study using spin-lock frequencies between 0-2500 Hz at 2.95 T and 1000 Hz at 7.05 T and found that dipolar interaction between water molecules and orientated collagen fibres is the main mechanism contributing to $R_{1\rho}$ values. They also proposed that dipolar interaction is the reason behind the correlation between $T_{1\rho}$ times and proteoglycan content in cartilage. In our experiment, a dispersive effect would vanish in

nearly all series at 50-100 Hz. The only series where the effect caused by the spin-lock pulse can be seen past 50 Hz is the 60 mg/g collagen concentration series. This suggests that the dispersion effect could only be visible in higher collagen concentrations, which are closer to the naturally occurring ones in articular cartilage.

Our study had some limitations. First, the orientation of the collagen fibres was uncontrolled in the gel. Fibre orientation has been shown in previous studies to influence the appearance of cartilage samples in MR images and the relaxation properties of articular cartilage [6], [8]; Mosher et al. [50] studied the magic angle effect on T_2 values and found that T_2 relaxation times increase when cartilage samples are placed at the "magic angle" compared with parallel to the external field, and that the effect is more noticeable at the more superficial layers of cartilage compared to the radial layer. Mlynárik et al. [49] found that $R_{1\rho}$ relaxation rates at 2.95 T and 7.05 with SLF between 0 and 2500 Hz were less influenced by the orientation of the sample and fibre orientation compared to R_2 values. Akella et al. [51] found that the laminar appearance seen in T_2 images when the cartilage sample was not placed at the "magic angle" orientation was removed using $T1\rho$ sequences at 4.7 T with a spin-lock frequency over 500 Hz. In our study, however, the magic angle effect was mitigated by the gels being isotropic, since we were interested in the fundamental effects of the substances themselves on relaxation.

Some of the samples had issues with gel uniformity, as some air bubbles were inadvertently created into the samples during the mixing process. $R_{1\rho}$ values were only obtained at 9.4 T, due to technical limitations at lower magnetic fields during the imaging process, so a comparison between $R_{1\rho}$ values at different B_0 could not be achieved. A further limitation could be that the collagen and CS concentrations were not quantified chemically after creating the phantoms, e.g. by measuring the hydroxyproline content of the samples in order to quantify collagen amounts in the gels.

In conclusion, in our collagen gel phantoms R_1 values generally increased by increasing collagen concentration at magnetic fields commonly used in clinical MR imaging, like 1.5 T and 3.0 T. However, no apparent increase was seen with varying chondroitin sulfate concentrations. R_2 values were also nearly unaffected at lower magnetic fields by concentration variations, although grew with chondroitin sulfate concentration at high magnetic fields, such as 9.4 T. $R_{1\rho}$ could also be used as an indicator on the amounts of collagen or chondroitin sulfate, since the values changed by varying the concentrations of either substance.

Bibliography

[1] Y. Zhang and J. M. Jordan. "Epidemiology of Osteoarthritis". In: *Clinics in Geriatric Medicine* 26.3 (2010), pp. 355–369. DOI: 10.1016/j.cger.2010.03.001.

[2] R. C. Lawrence, D. T. Felson, C. G. Helmick, et al. "Estimates of the prevalence of arthritis and other rheumatic conditions in the United States: Part II". In: *Arthritis & Rheumatism* 58.1 (2008), pp. 26–35. DOI: 10.1002/art.23176.

[3] Working group appointed by the Finnish Medical Society Duodecim and the Finnish Orthopaedic Association, Helsinki: The Finnish Medical Society Duodecim. *Polvi- ja lonkkanivelrikko*. Finnish. 2018. URL: www.kaypahoito.fi/hoi50054 (visited on 03/19/2020).

[4] M. Hiligsmann, C. Cooper, N. Arden, et al. "Health economics in the field of osteoarthritis: An Expert's consensus paper from the European Society for Clinical and Economic Aspects of Osteoporosis and Osteoarthritis (ESCEO)". In: *Seminars in Arthritis and Rheumatism* 43.3 (2013), pp. 303–313. DOI: 10.1016/j.semarthrit.2013.07.003.

[5] D. A. Reiter, P.-C. Lin, K. W. Fishbein, and R. G. Spencer. "Multicomponent T2 relaxation analysis in cartilage". In: *Magnetic Resonance in Medicine* 61.4 (2009), pp. 803–809. DOI: 10.1002/mrm.21926.

[6] Y. Xia. "Relaxation anisotropy in cartilage by NMR microscopy (μMRI) at 14-μm resolution". In: *Magnetic Resonance in Medicine* 39.6 (1998), pp. 941–949. DOI: 10.1002/mrm.1910390612.

[7] M. T. Nieminen, J. Töyräs, J. Rieppo, J. M. Hakumäki, J. Silvennoinen, H. J. Helminen, and J. S. Jurvelin. "Quantitative MR microscopy of enzymatically degraded articular cartilage". In: *Magnetic Resonance in Medicine* 43.5 (2000), pp. 676–681. DOI: 10.1002/(SICI)1522-2594(200005)43:5<676::AID-MRM9>3.0.CO;2-X.

[8] N. Hänninen, J. Rautiainen, L. Rieppo, S. Saarakkala, and M. J. Nissi. "Orientation anisotropy of quantitative MRI relaxation parameters in ordered tissue". In: *Scientific Reports* 7.1 (2017). DOI: 10.1038/s41598-017-10053-2.

[9] Y.-X. J. Wáng, Q. Zhang, X. Li, W. Chen, A. Ahuja, and J. Yuan. "T1ρ magnetic resonance: basic physics principles and applications in knee and intervertebral disc imaging". In: *Quantitative Imaging in Medicine and Surgery* 5.6 (2015). DOI: 10.3978/j.issn.2223-4292.2015.12.06.

[10] U. Duvvuri, A. D. Goldberg, J. K. Kranz, et al. "Water Magnetic Relaxation Dispersion in Biological Systems: The Contribution of Proton Exchange and Implications for the Noninvasive Detection of Cartilage Degradation". English. In: *Proceedings of the National Academy of Sciences of the United States of America* 98.22 (2001), pp. 12479–12484. DOI: 10.1073/pnas.221471898.

[11] L. C. Dijkgraaf, L. G. M. de Bont, G. Boering, and R. S. B. Liem. "The structure, biochemistry, and metabolism of osteoarthritic cartilage: A review of the literature". In: *Journal of Oral and Maxillofacial Surgery* 53.10 (1995), pp. 1182–1192. DOI: 10.1016/0278-2391(95)90632-0.

[12] R. R. Regatte, S. V. S. Akella, A. Borthakur, J. B. Kneeland, and R. Reddy. "Proteoglycan Depletion-Induced Changes in Transverse Relaxation Maps of Cartilage: Comparison of T2 and T1rho." English. In: *Academic Radiology* 9.12 (2002), pp. 1388–1394. DOI: 10.1016/S1076-6332(03)80666-9.

[13] N. M. Menezes, M. L. Gray, J. R. Hartke, and D. Burstein. "T2 and T1rho MRI in articular cartilage systems". English. In: *Magnetic Resonance in Medicine* 51.3 (2004), pp. 503–509. DOI: 10.1002/mrm.10710.

[14] X. Li, J. Cheng, K. Lin, et al. "Quantitative MRI using T1ρ and T2 in human osteoarthritic cartilage specimens: correlation with biochemical measurements and histology". In: *Magnetic Resonance Imaging* 29.3 (2011), pp. 324–334. DOI: 10.1016/j.mri.2010.09.004.

[15] M. T. Nieminen, J. Töyräs, M. S. Laasanen, J. Silvennoinen, H. J. Helminen, and J. S. Jurvelin. "Prediction of biomechanical properties of articular cartilage with quantitative magnetic resonance imaging". In: *Journal of Biomechanics* 37.3 (2004), pp. 321–328. DOI: 10.1016/S0021-9290(03)00291-4.

[16] C. Taylor, J. Carballido-Gamio, S. Majumdar, and X. Li. "Comparison of quantitative imaging of cartilage for osteoarthritis: T2, T1rho, dGEMRIC and contrast-enhanced computed tomography". English. In: *Magnetic resonance imaging* 27.6 (2009), pp. 779–784. DOI: 10.1016/j.mri.2009.01.016.

[17] J. C. Y. Hu and K. A. Athanasiou. "Structure and Function of Articular Cartilage". In: *Handbook of Histology Methods for Bone and Cartilage*. Ed. by Y. H. An and K. L. Martin. Totowa, N.J: Humana Press, 2003. Chap. 4, pp. 73–95. DOI: 10.1007/978-1-59259-417-7_4.

[18] D. Responte, R. Natoli, and K. Athanasiou. "Collagens of Articular Cartilage: Structure, Function, and Importance in Tissue Engineering". In: *Critical reviews in biomedical engineering* 35 (Feb. 2007), pp. 363–411. DOI: 10.1615/CritRevBiomedEng.v35.i5.20.

[19] M. Huber, S. Trattnig, and F. Lintner. "Anatomy, Biochemistry, and Physiology of Articular Cartilage". In: *Investigative radiology* 35.10 (2000). DOI: 10.1097/00004424-200010000-00003.

[20] B. Brodsky and A. V. Persikov. "Molecular Structure of the Collagen Triple Helix". In: *Fibrous Proteins: Coiled-Coils, Collagen and Elastomers*. Vol. 70. Advances in Protein Chemistry. Academic Press, 2005, pp. 301–339. DOI: https://doi.org/10.1016/S0065-3233(05)70009-7.

[21] K. E. Kadler, C. Baldock, J. Bella, and R. P. Boot-Handford. "Collagens at a glance". In: *Journal of Cell Science* 120.12 (2007), pp. 1955–1958. DOI: 10.1242/jcs.03453. eprint: https://jcs.biologists.org/content/120/12/1955.full.pdf.

[22] C. Knupp and J. M. Squire. "Molecular Packing in Network-Forming Collagens". In: *The Scientific World JOURNAL* 3 (2003), pp. 558–577. DOI: 10.1100/tsw.2003.40. Figure licensed under CC BY 3.0 via ResearchGate.

[23] Y. Xia. "Magic-Angle Effect in Magnetic Resonance Imaging of Articular Cartilage". In: *Investigative Radiology* 35.10 (2000), pp. 602–621. DOI: 10.1097/00004424-200010000-00007.

[24] R. Kijowski and R. Chaudhary. "Quantitative Magnetic Resonance Imaging of the Articular Cartilage of the Knee Joint". In: *Magnetic Resonance Imaging Clinics of North America* 22.4 (2014). MRI of the Knee, pp. 649–669. DOI: https://doi.org/10.1016/j.mric.2014.07.005.

[25] M. T. Bayliss, M. Venn, A. Maroudas, and S. Y. Ali. "Structure of proteoglycans from different layers of human articular cartilage". In: *Biochemical Journal* 209.2 (Feb. 1983), pp. 387–400. DOI: 10.1042/bj2090387.

[26] T. C. Dunn, Y. Lu, H. Jin, M. D. Ries, and S. Majumdar. "T2 Relaxation Time of Cartilage at MR Imaging: Comparison with Severity of Knee Osteoarthritis". In: *Radiology* 232.2 (2004), pp. 592–598. DOI: 10.1148/radiol.2322030976.

[27] M. L. Gray, D. Burstein, Y.-J. Kim, and A. Maroudas. "Magnetic resonance imaging of cartilage glycosaminoglycan: Basic principles, imaging technique, and clinical applications". In: *Journal of Orthopaedic Research* 26.3 (2008), pp. 281–291. DOI: 10.1002/jor.20482.

[28] A. Borthakur, E. Mellon, S. Niyogi, W. Witschey, J. B. Kneeland, and R. Reddy. "Sodium and T1ρ MRI for molecular and diagnostic imaging of articular cartilage". In: *NMR in Biomedicine* 19.7 (2006), pp. 781–821. DOI: 10.1002/nbm.1102.

[29] R. W. Brown, M. R. Thompson, R. Venkatesan, Y.-C. N. Cheng, and E. M. Haacke. *Magnetic Resonance Imaging: Physical Principles and Sequence Design.* Vol. 2. Wiley-Blackwell, 2014.

[30] D. J. Dowsett, P. A. Kenny, and R. E. Johnston. *The Physics of Diagnostic Imaging.* 2nd ed. Hodder Arnold, 2006.

[31] D. W. McRobbie, E. A. Moore, M. J. Graves, and M. R. Prince. *MRI from Picture to Proton.* 2nd ed. Cambridge University Press, 2006. DOI: 10.1017/CBO9780511545405.

[32] F. Bloch. "Nuclear Induction". In: *Phys. Rev.* 70 (7-8 Oct. 1946), pp. 460–474. DOI: 10.1103/PhysRev.70.460.

[33] S. H. Koenig and W. E. Schillinger. "Nuclear Magnetic Relaxation Dispersion in Protein Solutions: I. APOTRANSFERRIN". In: *Journal of Biological Chemistry* 244.12 (1969), pp. 3283–3289. eprint: http://www.jbc.org/content/244/12/3283.

[34] S. H. Koenig. "Molecular basis of magnetic relaxation of water protons of tissue". In: *Academic Radiology* 3.7 (1996), pp. 597–606. DOI: 10.1016/S1076-6332(96)80225-X.

[35] R. G. Bryant. "The dynamics of water-protein interactions." In: *Annual Review of Biophysics and Biomolecular Structure* 25.1 (1996), pp. 29–53. DOI: 10.1146/annurev.bb.25.060196.000333.

[36] U. Duvvuri, R. Reddy, S. D. Patel, J. H. Kaufman, J. B. Kneeland, and J. S. Leigh. "T(1rho)-relaxation in articular cartilage: Effects of enzymatic degradation". English. In: *Magnetic Resonance in Medicine* 38.6 (1997), pp. 863–867. DOI: 10.1002/mrm.1910380602.

[37] S. V. S. Akella, R. R. Regatte, A. J. Gougoutas, et al. "Proteoglycan induced changes in T1rho relaxation of articular cartilage at 4T". English. In: *Magnetic Resonance in Medicine* 46.3 (2001), pp. 419–423. DOI: 10.1002/mrm.1208.

[38] C. J. Westover and M. H. Dresden. "Collagen hydration: Pulsed nuclear magnetic resonance studies of structural transitions". In: *Biochimica et Biophysica Acta (BBA) - Protein Structure* 365.2 (1974), pp. 389–399. DOI: 10.1016/0005-2795(74)90011-7.

[39] H. T. Edzes and E. T. Samulski. "Cross relaxation and spin diffusion in the proton NMR of hydrated collagen". In: *Nature* 265 (1977), pp. 521–523. DOI: 10.1038/265521a0.

[40] A. Watanabe, C. Boesch, T. Obata, and S. E. Anderson. "Effect of multislice acquisition on T1 and T2 measurements of articular cartilage at 3T". In: *Journal of Magnetic Resonance Imaging* 26.1 (2007), pp. 109–117. DOI: 10.1002/jmri.20962.

[41] M. Takeuchi, M. Sekino, N. Iriguchi, and S. Ueno. "Dependence of the Spin-Spin Relaxation Time of Water in Collagen Gels on Collagen Fiber Directions". In: *Magnetic Resonance in Medical Sciences* 3.4 (2004), pp. 153–157. DOI: 10.2463/mrms.3.153.

[42] H. Kudo, N. Mukai, C. Gouping, et al. "The evaluation of collagen gel with various connection states by using MRI". In: *Materials Science and Engineering C* 28.2 (2008), pp. 270–273. DOI: 10.1016/j.msec.2006.10.012.

[43] A. Virta, M. Komu, and M. Kormano. "T1rho of protein solutions at very low fields: Dependence on molecular weight, concentration, and structure". In: *Magnetic Resonance in Medicine* 37.1 (1997), pp. 53–57. DOI: 10.1002/mrm.1910370109.

[44] *Instructions: Collagen Type I, rat tail, 5 mg/ml*. English. Version 2.2. ibidi GmbH. Sept. 18, 2019. URL: https://ibidi.com/img/cms/products/cells_reagents/R_5020X_CollagenI/IN_5020X_CollagenI_05mg.pdf (visited on 04/09/2020).

[45] W. R. Witschey, A. Borthakur, M. A. Elliott, E. Mellon, S. Niyogi, C. Wang, and R. Reddy. "Compensation for spin-lock artifacts using an off-resonance rotary echo in T1rho off-weighted imaging". In: *Magnetic Resonance in Medicine* 57.1 (2007), pp. 2–7. DOI: 10.1002/mrm.21134.

[46] J. Yin, Y. Xia, and M. Lu. "Concentration profiles of collagen and proteoglycan in articular cartilage by Fourier transform infrared imaging and principal component regression". In: *Spectrochimica Acta Part A Molecular and Biomolecular Spectroscopy* 88 (2012), pp. 90–96. DOI: 10.1016/j.saa.2011.12.002.

[47] E. Wiener, C. W. A. Pfirrmann, and J. Hodler. "Spatial variation in T1 of healthy human articular cartilage of the knee joint". In: *British Journal of Radiology* 83.990 (2010), pp. 476–485. DOI: 10.1259/bjr/62779246.

[48] E. Lammentausta, P. Kiviranta, M. Nissi, M. Laasanen, I. Kiviranta, M. Nieminen, and J. Jurvelin. "T2 relaxation time and delayed gadolinium-enhanced MRI of cartilage (dGEMRIC) of human patellar cartilage at 1.5 T and 9.4 T: Relationships with tissue mechanical properties". In: *Journal of Orthopaedic Research* 24.3 (2006), pp. 366–374. DOI: 10.1002/jor.20041.

[49] V. Mlynárik, P. Szomolányi, R. Toffanin, F. Vittur, and S. Trattnig. "Transverse relaxation mechanisms in articular cartilage". English. In: *Journal of Magnetic Resonance* 169.2 (2004), pp. 300–307. DOI: 10.1016/j.jmr.2004.05.003.

[50] T. J. Mosher, H. Smith, B. J. Dardzinski, V. J. Schmithorst, and M. B. Smith. "MR Imaging and T2 Mapping of Femoral Cartilage: In Vivo Determination of the Magic Angle Effect." In: *American Journal of Roentgenology* 177.3 (2001), pp. 665–669. DOI: 10.2214/ajr.177.3.1770665.

[51] S. V. S. Akella, R. R. Regatte, A. J. Wheaton, A. Borthakur, and R. Reddy. "Reduction of residual dipolar interaction in cartilage by spin lock technique". English. In: *Magnetic Resonance in Medicine* 52.5 (2004), pp. 1103–1109. DOI: 10.1002/mrm.20241.